Eur. Phys. J. C (2022) 82:667
https://doi.org/10.1140/epjc/s10052-022-10590-9

THE EUROPEAN PHYSICAL JOURNAL C

Regular Article - Theoretical Physics

Loop-corrected Higgs masses in the NMSSM with inverse seesaw mechanism

Thi Nhung Dao[1,2,a], **Margarete Mühlleitner**[3,b], **Anh Vu Phan**[2,4,5,c]

[1] Faculty of Fundamental Sciences, PHENIKAA University, Hanoi 12116, Vietnam
[2] Institute For Interdisciplinary Research in Science and Education, ICISE, Quy Nhon 590000, Vietnam
[3] Institute for Theoretical Physics, Karlsruhe Institute of Technology, Wolfgang-Gaede-Str. 1, 76131 Karlsruhe, Germany
[4] University of Science, Ho Chi Minh City, Vietnam
[5] Vietnam National University, Ho Chi Minh City, Vietnam

Received: 7 September 2021 / Accepted: 7 July 2022

Abstract In this study, we work in the framework of the Next-to-Minimal extension of the Standard Model (NMSSM) extended by six singlet leptonic superfields. Through the mixing with the three doublet leptonic superfields, the non-zero tiny neutrino masses can be generated through the inverse seesaw mechanism. While R-parity is conserved in this model lepton number is explicitly violated. We quantify the impact of the extended neutrino sector on the NMSSM Higgs sector by computing the complete one-loop corrections with full momentum dependence to the Higgs boson masses in a mixed on-shell-$\overline{\text{DR}}$ renormalization scheme, with and without the inclusion of CP violation. The results are consistently combined with the dominant two-loop corrections at $\mathcal{O}(\alpha_t(\alpha_s+\alpha_t))$ to improve the predictions for the Higgs mixing and the loop-corrected masses. In our numerical study we include the constraints from the Higgs data, the neutrino oscillation data, the charged lepton flavor-violating decays $l_i \to l_j + \gamma$, and the new physics constraints from the oblique parameters S, T, U. We present in this context the one-loop decay width for $l_i \to l_j + \gamma$. The loop-corrected Higgs boson masses are included in the Fortran code `NMSSMCALC-nuSS`.

1 Introduction

Both cosmological and neutrino oscillation data have indicated the existence of three neutrino flavors, non-zero neutrino masses, and neutrino mixing. The three observed neutrinos are called active neutrinos. Cosmological data constrain the sum of the three active neutrino masses to be below 0.12 eV [1]. Their absolute values must hence be less than 0.12 eV. As a result, the effect from the three active neutrinos on the Higgs sector is negligible. However, models with an extended neutrino sector contain three active neutrinos and at least one sterile neutrino. The sterile neutrino can mix with the active neutrinos and help to explain the tininess of the active neutrino masses through the seesaw mechanism. The number of sterile neutrinos and their masses are model dependent. Current experiments have not observed sterile neutrinos yet but still allow for a small mixing between sterile and active neutrinos. For precise investigations and meaningful interpretations of both the Higgs and the neutrino sector, it is therefore worthwhile and mandatory to consider the effects of these sterile neutrinos on the Higgs sector. With the increasing amount of the experimental LHC data on the Higgs mass, couplings, production, and decay processes, one can expect stronger constraints on new physics affecting directly and/or indirectly the Higgs sector.

In this study, we consider the impact on the Higgs boson masses in a supersymmetric theory. More specifically, we work in the framework of the Next-to-Minimal Supersymmetric extension of the Standard Model (NMSSM) [2–17] with a Higgs sector consisting of two complex Higgs doublets and a complex Higgs singlet. After electroweak symmetry breaking (EWSB), the NMSSM Higgs sector features seven Higgs bosons, five neutral and two charged Higgs bosons. One of the neutral Higgs states is identified with the Standard Model (SM) Higgs boson. In the minimal supersymmetric extension of the SM (MSSM) its mass is bounded to be below the Z boson mass so that substantial radiative Higgs mass corrections are required to shift the tree-level mass value to the 125 GeV observed by the LHC experiments ATLAS [18] and CMS [19]. In the NMSSM, there is an additional contribution to the tree-level mass arising

[a] e-mail: nhung.daothi@phenikaa-uni.edu.vn (corresponding author)
[b] e-mail: margarete.muehlleitner@kit.edu
[c] e-mail: phananhvu1609@gmail.com

Published online: 03 August 2022

from the Higgs doublets mixing with the additional complex singlet, so that less substantial radiative corrections are required in order to comply with experiment. The neutrino sector in this model is extended to include six singlet leptonic superfields. R-parity is conserved while the lepton number is explicitly violated by an interaction term between two singlet neutrino superfields and a singlet Higgs superfield. This type of model was first discussed in [20]. The six singlet neutrinos mix with the three doublet ones to generate nine neutrino mass eigenstates. Three of them have very light masses, that can be explained through the inverse seesaw mechanism [21–23]. The six remaining neutrinos can have masses of order TeV which may be observable in collider experiments. The presence of heavy neutrinos allows the neutrino Yukawa couplings to be large. Hence heavy neutrinos and their superpartners loops can give significant contributions to loop-corrected Higgs boson masses even though their mixings with active neutrinos are small. This is the focus of our study.

In the literature, there exist many studies on the effects of the (s)neutrinos on the loop-corrected Higgs boson masses in the context of a supersymmetric theory with the type I or inverse seesaw mechanism. We briefly review here those studies that are close to our subject. The impact of the extended neutrino and sneutrino sector on the lightest CP-even Higgs mass in the NMSSM with the inverse seesaw mechanism (ISS), was presented in [24] using an approximate one-loop correction neglecting the effects from external momentum dependence and mixings between Higgs bosons. The authors of [25] have computed the one-loop corrections stemming solely from the neutrino/sneutrino sector to the lightest CP-even Higgs boson in the NMSSM extended by a right-handed neutrino superfield with R-parity conservation. The full one-loop corrections to neutral Higgs boson masses were presented in a mixed on-shell (OS)-$\overline{\text{DR}}$ scheme for the $\mu\nu$SSM model with only one generation in [26] and for three generations of right-handed neutrinos in [27]. In the $\mu\nu$SSM, the Higgs sector contains two Higgs doublets while the neutrino sector is extended to include singlet right-handed neutrino superfields. Lepton number and R-parity are not protected in the $\mu\nu$SSM so that the superpartners of the singlet right-handed neutrinos can develop vacuum expectation values (VEVs). In the Minimal Supersymmetric Standard Model (MSSM) extended by the type I seesaw mechanism, the full one-loop corrections with full momentum dependence combined with the dominant two-loop corrections to the Higgs boson masses were presented in [28], which showed a non-decoupling effect for a large right-handed neutrino scale. The authors of [29] have shown that the decoupling property is preserved with a suitable renormalization scheme of the parameter $\tan\beta$, which denotes the ratio of the two vacuum expectation values of the two Higgs doublets in the MSSM. With the inverse seesaw mechanism incorporated in the MSSM, the one-loop corrections of (s)neutrinos have been studied in [30,31] by using the one-loop effective potential approach.

Our goal is to present here the complete one-loop corrections with full momentum dependence to the Higgs boson masses in a mixed OS-$\overline{\text{DR}}$ renormalization scheme using the Feynman diagrammatic approach. The calculation has been done both in the real and the complex NMSSM. We consistently combine our result with the dominant two-loop corrections of $\mathcal{O}(\alpha_s\alpha_t)$ [32] and $\mathcal{O}(\alpha_t^2)$ [33] computed by our group. In order to investigate the impact of our newly computed corrections, we perform a numerical study where we apply constraints from the Higgs data, the neutrino oscillation data, the charged lepton flavor-violating decays $l_i \to l_j + \gamma$, and the constraints on new physics from the oblique parameters S, T, U. The explicit computation of the one-loop decay width for $l_i \to l_j + \gamma$ is also presented in this study. We furthermore provide the Fortran code, dubbed `NMSSMCALC-nuSS`, for the computation of the loop-corrected Higgs boson masses and Higgs boson decay branching ratios incorporating higher-order corrections. This code is adapted from the code `NMSSMCALC` [34] published by our group.[1]

The paper is organized as follows. In Sect. 2, we describe the model and the masses and mixings of each sector at tree level. In Sect. 3, we present details of our calculation of the loop-corrected Higgs boson masses and mixing. We also discuss our renormalization scheme for parameters and fields needed to obtain finite renormalized Higgs self-energies. In Sect. 4 we present all constraints related to the Higgs data, the neutrino oscillation data, the oblique parameters S, T, U, and the charged lepton flavor-violating decays $l_i \to l_j + \gamma$ that we apply in our phenomenological study. Section 5 is dedicated to the numerical analysis. We present the size of the loop corrections and their dependencies on the parameters of the neutrino and sneutrino sectors. We furthermore discuss the effects of different constraints on the neutrino sector parameters. Finally, we present our conclusions in Sect. 6.

2 The NMSSM with inverse seesaw mechanism

The NMSSM realization of the seesaw mechanism through the $\mathbb{Z}_3$ discrete symmetry with a unit charge of $\omega = e^{i2\pi/3}$ has been introduced in [20,24]. Depending on the $\mathbb{Z}_3$ charge assignment for the lepton doublet superfields and the two Higgs doublet superfields, the neutrino masses may arise from effective dimension five, six or seven operators. We consider in this paper the case of the dimension six operator. Tiny

[1] Our recently published code `NMSSMCALCEW` also includes the supersymmetric (SUSY) electroweak [35] and SUSY-QCD corrections to the NMSSM Higgs boson decay widths and branching ratios [36].

Table 1 Quantum numbers associated with the gauge symmetry group $SU(2)_L$, $U(1)_Y$, the $\mathbb{Z}_3$ charge ($\omega = e^{i2\pi/3}$) and the lepton number L for the NMSSM superfields. The generation index i runs from one to three

	$SU(2)_L$	$U(1)_Y$	Z_3	L
$\hat{Q}_i$	2	1/3	1	0
$\hat{U}_i^c$	1	− 4/3	ω^2	0
$\hat{D}_i^c$	1	2/3	ω^2	0
$\hat{L}_i$	2	− 1	1	1
$\hat{E}_i^c$	1	2	ω^2	− 1
$\hat{H}_u$	2	1	ω	0
$\hat{H}_d$	2	− 1	ω	0
$\hat{S}$	1	0	ω	0
$\hat{N}_i^c$	1	0	ω^2	− 1
$\hat{X}_i$	1	0	ω	1

neutrino masses are obtained through the well-known inverse seesaw mechanism. This is an interesting case because the dimension six operators generating neutrino masses are not present in the non-supersymmetric seesaw models.[2] Another reason that makes this case more interesting is that the new appearing particles need not to be too heavy in order to obtain tiny masses for the observed neutrinos. They can be at the TeV scale and hence in the reach of present and future colliders. We consider the simple case where we introduce six gauge singlet chiral superfields, $\hat{N}_i$, $\hat{X}_i$ ($i = 1, 2, 3$). These superfields carry lepton number. The $\mathbb{Z}_3$ charge assignment[3] used in this paper for the relevant NMSSM superfields is given in Table 1.

The NMSSM superpotential including the new superfields is given by

$$W_{\rm NMSSM} = W_{\rm MSSM} - \epsilon_{ab}\lambda \hat{S}\hat{H}_d^a\hat{H}_u^b + \frac{1}{3}\kappa\hat{S}^3 - y_\nu\epsilon_{ab}\hat{H}_u^a\hat{L}^b\hat{N}^c + \lambda_X\hat{S}\hat{X}\hat{X} + \mu_X\hat{X}\hat{N}^c, \quad (2.1)$$

where ϵ_{ab} is the totally antisymmetric tensor with $\epsilon_{12} = \epsilon^{12} = 1$, $\hat{H}_u$, $\hat{H}_d$ denote the two complex Higgs doublet superfields and $\hat{S}$ the complex singlet superfield. The MSSM superpotential reads

$$W_{\rm MSSM} = -\epsilon_{ab}\big(y_u\hat{H}_u^a\hat{Q}^b\hat{U}^c - y_d\hat{H}_d^a\hat{Q}^b\hat{D}^c - y_e\hat{H}_d^a\hat{L}^b\hat{E}^c\big), \quad (2.2)$$

in terms of the left-handed quark and lepton superfield doublets $\hat{Q}$ and $\hat{L}$ and the right-handed up-type, down-type and electron-type superfield singlets $\hat{U}$, $\hat{D}$ and $\hat{E}$, respectively. Charge conjugation is denoted by the superscript c, and color and generation indices have been omitted. The NMSSM superpotential contains the coupling κ of the self-interaction of the singlet superfield $\hat{S}$, the coupling λ for the $\hat{S}$ interaction with the two Higgs doublet superfields, and the coupling λ_X for the interaction of the Higgs singlet with the two singlets $\hat{X}$. In general, the coupling λ_X is a 3×3 matrix. This is the only term in the superpotential that violates the lepton number. Note that in the model we consider here, we allow for explicit lepton number violation, however, we consider only the violation of two units ($\Delta L = 2$). This will forbid the nine scalar fields that carry lepton number to develop VEVs. As consequence, lepton number violation appears only in the (s)neutrino sector and we stay in the simplest possible parameter space. The 3×3 matrix μ_X is the only parameter with the dimension of mass in the superpotential so that it can be of the order of the SUSY conserving mass scale and is naturally large. This is essential for the seesaw mechanism. The quark and lepton Yukawa couplings y_d, y_u, y_e, y_ν and the couplings $\lambda, \kappa, \lambda_X, \mu_X$ are in general complex. In the numerical analysis, we chose y_d, y_u, y_e, λ_X, μ_X to be diagonal. However in the code λ_X, μ_X can be chosen to be non-diagonal. The soft SUSY breaking NMSSM Lagrangian respecting the gauge symmetry and the $\mathbb{Z}_3$ symmetry reads

$$\mathcal{L}^{\rm soft}_{\rm NMSSM} = \mathcal{L}^{\rm soft}_{\rm MSSM} - \tilde{m}_S^2|S|^2 + \Big(\epsilon_{ab}A_\lambda\lambda S H_d^a H_u^b - \frac{1}{3}A_\kappa\kappa S^3 + \epsilon_{ab}y_\nu A_\nu H_u^a\tilde{L}^b\tilde{N}^* + \lambda_X A_X S\tilde{X}\tilde{X} + \mu_X B_{\mu_X}\tilde{X}\tilde{N}^* + h.c.\Big) - \tilde{m}_X^2|\tilde{X}|^2 - \tilde{m}_N^2|\tilde{N}|^2, \quad (2.3)$$

and contains the soft SUSY breaking trilinear couplings A_λ, A_κ, A_ν and A_X, the soft SUSY breaking masses $\tilde{m}_S^2$, $\tilde{m}_X^2$, $\tilde{m}_N^2$ and the soft SUSY breaking bilinear mass B_{μ_X}. In general, A_λ, A_κ, A_ν, A_X and B_{μ_X} are complex parameters. For simplicity, in our numerical analysis we chose $\tilde{m}_X, \tilde{m}_N, A_X$, and B_{μ_X} to be diagonal. The SM-type and SUSY fields corresponding to a superfield (denoted with a hat) are represented by a letter without and with a tilde, respectively. The soft SUSY breaking MSSM contribution can be cast into the form

$$\mathcal{L}^{\rm soft}_{\rm MSSM} = -\tilde{m}_{H_d}^2|H_d|^2 - \tilde{m}_{H_u}^2|H_u|^2 - \tilde{m}_Q^2|\tilde{Q}|^2 - \tilde{m}_U^2|\tilde{u}_R|^2 - \tilde{m}_D^2|\tilde{d}_R|^2 - \tilde{m}_L^2|\tilde{L}|^2 - \tilde{m}_E^2|\tilde{e}_R|^2 + \epsilon_{ab}\Big(y_u A_u H_u^a\tilde{Q}^b\tilde{u}_R^* - y_d A_d H_d^a\tilde{Q}^b\tilde{d}_R^* - y_e A_e H_d^a\tilde{Q}^b\tilde{e}_R^* + h.c.\Big) - \frac{1}{2}(M_1\tilde{B}\tilde{B} + M_2\tilde{W}_i\tilde{W}_i + M_3\tilde{G}\tilde{G} + h.c). \quad (2.4)$$

[2] In non-supersymmetric seesaw models, effective dimension five operators give masses for light neutrinos while dimension six operators affect their kinetic terms.

[3] Other assignments of the $\mathbb{Z}_3$ charge were also discussed in [20].

The indices of the soft SUSY breaking masses, Q (L), stand for the left-handed doublet of the three quark (lepton) generations, and U, D, E are the indices for the right-handed up-type and down-type quarks and charged leptons, respectively. In the trilinear coupling parameters, the indices u, d, e represent the up-type and down-type quarks and charged leptons. While the trilinear couplings A_u, A_d and A_e are complex, the soft SUSY breaking mass terms $\tilde{m}_x^2$ ($x = S, H_u, H_d, Q, U, D, L, E$) are real. The soft SUSY breaking mass parameters of the gauginos, M_1, M_2, M_3, for the bino, the winos and the gluinos, $\tilde{B}$, $\tilde{W}_i$ ($i = 1, 2, 3$) and $\tilde{G}$, corresponding to the weak hypercharge $U(1)_Y$, the weak isospin $SU(2)_L$ and the colour $SU(3)_C$ symmetry, are in general complex. In this paper we are working in complex NMSSM where the parameters are kept complex. Furthermore, we apply flavor conservation in the charged (s)lepton and (s)quark sectors so that all matrices including soft mass matrices $\tilde{m}_L^2, \tilde{m}_E^2, \tilde{m}_Q^2, \tilde{m}_U^2, \tilde{m}_D^2$, the trilinear couplings $A_{e,d,u}$ and the Yukawa matrices $Y_{e,d,u}$ are diagonal in any basis. Flavor mixing occurring in our model arises solely from the neutrino and sneutrino sectors. The Lagrangian contains two lepton number violating terms, namely $\lambda_X \hat{S}\hat{X}\hat{X}$ and $\lambda_X A_X S\tilde{X}\tilde{X}$.

The Higgs, neutralino, chargino, (s)quark and charged (s)lepton sectors are the same as in the usual NMSSM without seesaw. For completeness, we recall briefly these sectors here to introduce our notation. The sectors that receive significant changes are the neutrino and sneutrino ones. We will present them in detail later on. Expanding the scalar Higgs fields about their vacuum expectation values (VEVs) v_u, v_d, and v_s, we have

$$\begin{aligned} H_d &= \begin{pmatrix} \frac{1}{\sqrt{2}}(v_d + h_d + ia_d) \\ h_d^- \end{pmatrix}, \\ H_u &= e^{i\varphi_u} \begin{pmatrix} h_u^+ \\ \frac{1}{\sqrt{2}}(v_u + h_u + ia_u) \end{pmatrix}, \\ S &= e^{i\varphi_s} \frac{1}{\sqrt{2}}(v_s + h_s + ia_s), \end{aligned} \tag{2.5}$$

where two additional complex phases, φ_u, φ_s, have been introduced. The fields h_i and a_i with $i = d, u, s$ correspond to the CP-even and CP-odd part, respectively, of the neutral entries of H_u, H_d and S. The charged components are denoted by $h_{d,u}^{\pm}$.

After EWSB, there are mixings between the three CP-even and the three CP-odd Higgs interaction states. In the basis $\phi = (h_d, h_u, h_s, a_d, a_u, a_s)$, the mass term is given by

$$\mathcal{L} = \frac{1}{2}\phi^T M_{\phi\phi}\phi. \tag{2.6}$$

The explicit expression of the mass matrix $M_{\phi\phi}$ can be found in [33]. The transformation into mass eigenstates at tree-level can be performed in two steps. First, $\mathcal{R}^G$ is used to single out the Goldstone boson whose mass is equal to the Z boson mass in the 't Hooft-Feynman gauge,

$$M_{hh}^{(6)} = \mathcal{R}^G M_{\phi\phi} \left(\mathcal{R}^G\right)^T, \tag{2.7}$$

$$(h_d, h_u, h_s, a, a_s, G)^T = \mathcal{R}^G (h_d, h_u, h_s, a_d, a_u, a_s)^T. \tag{2.8}$$

Here one can remove the Goldstone state from the rest by crossing out the sixth row and column of $M_{hh}^{(6)}$, so that it becomes a 5×5 mass matrix in the basis (h_d, h_u, h_s, a, a_s). In the second step, we diagonalize the thus obtained 5×5 matrix M_{hh} with an orthogonal matrix $\mathcal{R}$

$$\mathrm{diag}(m_{h_1}^2, m_{h_2}^2, m_{h_3}^2, m_{h_4}^2, m_{h_5}^2) = \mathcal{R} M_{hh} \mathcal{R}^T, \tag{2.9}$$

$$(h_1, h_2, h_3, h_4, h_5)^T = \mathcal{R}(h_d, h_u, h_s, a, a_s)^T. \tag{2.10}$$

The tree-level Higgs mass eigenstates are denoted by the small letter h. The masses are ordered as $m_{h_1} \leq m_{h_2} \leq m_{h_3} \leq m_{h_4} \leq m_{h_5}$.

The mass matrix in the 't Hooft-Feynman gauge for the charged components of the Higgs doublets,

$$\left(h_d^+, h_u^+\right) M_{h^+h^+} \begin{pmatrix} h_d^- \\ h_u^- \end{pmatrix}, \tag{2.11}$$

is given by

$$\begin{aligned} M_{h^+h^+} = \frac{1}{2} &\begin{pmatrix} t_\beta & 1 \\ 1 & 1/t_\beta \end{pmatrix} \\ &\times \left[M_W^2 s_{2\beta} + \frac{|\lambda| v_s}{\cos(\varphi_\lambda + \varphi_u + \varphi_s)} \left(\sqrt{2}\ \mathrm{Re} A_\lambda \right.\right. \\ &+ |\kappa| v_s \cos(\varphi_\kappa + 3\varphi_s)) \\ &\left.\left. - \frac{2|\lambda|^2 M_W^2 s_{\theta_W}^2}{e^2} s_{2\beta} \right] + M_W^2 \begin{pmatrix} {c_\beta}^2 & -c_\beta s_\beta \\ -c_\beta s_\beta & {s_\beta}^2 \end{pmatrix}, \end{aligned} \tag{2.12}$$

where M_W is the mass of the W boson, θ_W the electroweak mixing angle, e the electric charge and φ_λ, φ_κ the complex phases of λ and κ, respectively. The angle β is defined as

$$\tan\beta = \frac{v_u}{v_d}. \tag{2.13}$$

Here and in the following we use the short hand notation $c_x = \cos x$, $s_x = \sin x$ and $t_x = \tan x$. The mass matrix, $M_{h^+h^+}$, can be diagonalized by a rotation matrix with the angle $\beta_c = \beta$ leading to the charged Higgs mass given by

$$M_{H^\pm}^2 = M_W^2 + \frac{|\lambda| v_s}{s_{2\beta}\cos(\varphi_\lambda + \varphi_u + \varphi_s)} \times \left(\sqrt{2}\,\mathrm{Re}A_\lambda + |\kappa| v_s \cos(\varphi_\kappa + 3\varphi_s)\right) - \frac{2|\lambda|^2 M_W^2 s_{\theta_W}^2}{e^2}. \tag{2.14}$$

The mass of the charged Goldstone boson $G^\pm$ is equal to M_W.

The fermionic superpartners of the neutral Higgs bosons, $\tilde{H}_d^0$, $\tilde{H}_u^0$, $\tilde{S}$, and of the neutral gauge bosons, $\tilde{B}$, $\tilde{W}_3$, mix, and in the Weyl spinor basis $\psi^0 = (\tilde{B}, \tilde{W}_3, \tilde{H}_d^0, \tilde{H}_u^0, \tilde{S})^T$ the neutralino mass matrix M_N is given by

$$M_N = \begin{pmatrix} M_1 & 0 & -c_\beta M_Z s_{\theta_W} & M_Z s_\beta s_{\theta_W} e^{-i\varphi_u} & 0 \\ 0 & M_2 & c_\beta M_W & -M_W s_\beta e^{-i\varphi_u} & 0 \\ -c_\beta M_Z s_{\theta_W} & c_\beta M_W & 0 & -\lambda\frac{v_s}{\sqrt{2}} e^{i\varphi_s} & -\frac{\sqrt{2} M_W s_\beta s_{\theta_W} \lambda e^{i\varphi_u}}{e} \\ M_Z s_\beta s_{\theta_W} e^{-i\varphi_u} & -M_W s_\beta e^{-i\varphi_u} & -\lambda\frac{v_s}{\sqrt{2}} e^{i\varphi_s} & 0 & -\frac{\sqrt{2} M_W c_\beta s_{\theta_W} \lambda}{e} \\ 0 & 0 & -\frac{\sqrt{2} M_W s_\beta s_{\theta_W} \lambda e^{i\varphi_u}}{e} & -\frac{\sqrt{2} M_W c_\beta s_{\theta_W} \lambda}{e} & \sqrt{2}\kappa v_s e^{i\varphi_s} \end{pmatrix} \tag{2.15}$$

after EWSB, where M_Z is the Z boson mass. The neutralino mass matrix is symmetric and can be diagonalized by a 5×5 matrix N, yielding $\mathrm{diag}(m_{\tilde{\chi}_1^0}, m_{\tilde{\chi}_2^0}, m_{\tilde{\chi}_3^0}, m_{\tilde{\chi}_4^0}, m_{\tilde{\chi}_5^0}) = N^* M_N N^\dagger$, where the mass values are ordered as $m_{\tilde{\chi}_1^0} \leq \cdots \leq m_{\tilde{\chi}_5^0}$. The neutralino mass eigenstates $\tilde{\chi}_i^0$, expressed as a Majorana spinor, are then obtained by

$$\tilde{\chi}_i^0 = \begin{pmatrix} \chi_i^0 \\ \overline{\chi_i^0} \end{pmatrix} \quad \text{with} \quad \chi_i^0 = N_{ij}\psi_j^0, \quad i,\ j = 1,\ldots,5, \tag{2.16}$$

where

$$\overline{\chi_i^0} = i\sigma_2 \chi_i^{0*} \tag{2.17}$$

in terms of the Pauli matrix σ_2.

The fermionic superpartners of the charged Higgs and gauge bosons are given in terms of the Weyl spinors $\tilde{H}_d^\pm$, $\tilde{H}_u^\pm$, $\tilde{W}^-$, and $\tilde{W}^+$. With

$$\psi_R^- = \begin{pmatrix} \tilde{W}^- \\ \tilde{H}_d^- \end{pmatrix} \quad \text{and} \quad \psi_L^+ = \begin{pmatrix} \tilde{W}^+ \\ \tilde{H}_u^+ \end{pmatrix}, \tag{2.18}$$

the mass term for these spinors reads

$$\mathcal{L} = (\psi_R^-)^T M_C \psi_L^+ + h.c., \tag{2.19}$$

where

$$M_C = \begin{pmatrix} M_2 & \sqrt{2} s_\beta M_W e^{-i\varphi_u} \\ \sqrt{2} c_\beta M_W & \lambda\frac{v_s}{\sqrt{2}} e^{i\varphi_s} \end{pmatrix}. \tag{2.20}$$

The chargino mass matrix M_C can be diagonalized with the help of two unitary 2×2 matrices, U and V, resulting in

$$\mathrm{diag}(m_{\tilde{\chi}_1^\pm}, m_{\tilde{\chi}_2^\pm}) = U^* M_C V^\dagger, \tag{2.21}$$

with $m_{\tilde{\chi}_1^\pm} \leq m_{\tilde{\chi}_2^\pm}$. The left-handed and the right-handed part of the mass eigenstates are

$$\tilde{\chi}_L^+ = V\psi_L^+ \quad \text{and} \quad \tilde{\chi}_R^- = U\psi_R^-, \tag{2.22}$$

respectively, with the mass eigenstates ($i = 1, 2$)

$$\tilde{\chi}_i^+ = \begin{pmatrix} \tilde{\chi}_{L_i}^+ \\ \overline{\tilde{\chi}_{R_i}^-} \end{pmatrix} \tag{2.23}$$

written as Dirac spinors.

The scalar partners of the left- and right-handed quarks are denoted as $\tilde{q}_L$ and $\tilde{q}_R$, respectively. Assuming no generation mixing in the squark sector the mass matrix for the top squark in the interaction basis $(\tilde{t}_L, \tilde{t}_R)$ reads

$$M_{\tilde{t}} = \begin{pmatrix} m_{\tilde{Q}_3}^2 + m_t^2 + M_Z^2 c_{2\beta}(\frac{1}{2} - \frac{2}{3}s_{\theta_W}^2) & m_t\left(A_t^* e^{-i\varphi_u} - \mu_{\mathrm{eff}}/t_\beta\right) \\ m_t\left(A_t e^{i\varphi_u} - \mu_{\mathrm{eff}}{}^*/t_\beta\right) & m_t^2 + m_{\tilde{t}_R}^2 + \frac{2}{3}M_Z^2 c_{2\beta} s_{\theta_W}^2 \end{pmatrix}, \tag{2.24}$$

while the bottom squark mass matrix is given by

$$M_{\tilde{b}} = \begin{pmatrix} m_{\tilde{Q}_3}^2 + m_b^2 + M_Z^2 c_{2\beta}(-\frac{1}{2} + \frac{1}{3}s_{\theta_W}^2) & m_b\left(A_b^* - e^{i\varphi_u}\mu_{\mathrm{eff}} t_\beta\right) \\ m_b\left(A_b - e^{-i\varphi_u}\mu_{\mathrm{eff}}{}^* t_\beta\right) & m_b^2 + m_{\tilde{b}_R}^2 - \frac{1}{3}M_Z^2 c_{2\beta} s_{\theta_W}^2 \end{pmatrix}, \tag{2.25}$$

where

$$\mu_{\mathrm{eff}} = \frac{\lambda v_s e^{i\varphi_s}}{\sqrt{2}}. \tag{2.26}$$

The mass eigenstates are obtained by diagonalizing these squark matrices with the unitary transformations

$$\mathrm{diag}(m_{\tilde{q}_1}^2, m_{\tilde{q}_2}^2) = U_{\tilde{q}} M_{\tilde{q}} U_{\tilde{q}}^\dagger, \quad \begin{pmatrix} \tilde{q}_1 \\ \tilde{q}_2 \end{pmatrix} = U_{\tilde{q}} \begin{pmatrix} \tilde{q}_L \\ \tilde{q}_R \end{pmatrix}, q = t, b, \tag{2.27}$$

with the usual convention $m_{\tilde{q}_1} \leq m_{\tilde{q}_2}$.

For the charged leptonic sector, we use the same assumption of no generation mixing as in the squark sector. In each generation, the left- and right-handed sleptons mix. For example, the mixing matrix for the third generation, *i.e.* for the left- and right-handed stau, is given by

$$M_{\tilde{\tau}} = \begin{pmatrix} m^2_{\tilde{L}_3} + m^2_\tau + M^2_Z c_{2\beta}\left(-\frac{1}{2} + s^2_{\theta_W}\right) & m_\tau\left(A^*_\tau - e^{i\varphi_u}\mu_{\text{eff}} t_\beta\right) \\ m_\tau\left(A_\tau - e^{-i\varphi_u}\mu_{\text{eff}}{}^* t_\beta\right) & m^2_\tau + m^2_{\tilde{\tau}_R} - M^2_Z c_{2\beta} s^2_{\theta_W} \end{pmatrix}, \tag{2.28}$$

Upon diagonalization we obtain the mass eigenstates $\tilde{\tau}_1$ and $\tilde{\tau}_2$ whose masses are ordered as $m_{\tilde{\tau}_1} \leq m_{\tilde{\tau}_2}$.

In the neutral leptonic sector, the three left-handed neutrinos, ν_{L_i}, mix with the six leptonic component fields of the six singlet superfields $\hat{N}^c_i$, $\hat{X}_i$, $i = 1, 2, 3$, and the mass term in the Lagrangian reads

$$\mathcal{L}^\nu_{\text{mass}} = -\frac{1}{2}\begin{pmatrix} \nu_L & N^c & X \end{pmatrix} M^\nu_{\text{ISS}} \begin{pmatrix} \nu_L \\ N^c \\ X \end{pmatrix} \tag{2.29}$$

where the mixing mass matrix is given by

$$M^\nu_{\text{ISS}} = \begin{pmatrix} 0 & M_D & 0 \\ M^T_D & 0 & \mu_X \\ 0 & \mu^T_X & M_X \end{pmatrix}. \tag{2.30}$$

Note that ν_{L_i}, N^c_i, X_i are left-handed Weyl spinors and the products of them are defined in such a way that they are Lorentz invariant. For example, $\nu_{L_i} N^c_j = \epsilon^{ab}\nu_{L_i,a} N^c_{j,b}$, where the spinor indices are denoted by $a, b = 1, 2$, and the generation indices by $i, j = 1, 2, 3$. The blocks M_D, μ_X and M_X are 3×3 matrices with μ_X defined in Eq. (2.1) and

$$M_D = \frac{v_u e^{i\varphi_u}}{\sqrt{2}} y_\nu, \quad M_X = \frac{v_s e^{i\varphi_s}}{\sqrt{2}}(\lambda_X + \lambda^T_X). \tag{2.31}$$

The mass matrix M^ν_{ISS} can be diagonalized by a 9×9 unitary matrix as

$$U^*_\nu M^\nu_{\text{ISS}} U^\dagger_\nu = \text{diag}(m_{n_1}, \ldots, m_{n_9}). \tag{2.32}$$

The diagonalization process is done numerically in our code. It can be performed, however, by using an expansion approximation [37,38] to separate the 3×3 light neutrino mass matrix from the 6×6 heavy states exploiting the fact that all matrix elements of M_D, M_X are much smaller than the eigenvalues of μ_X. In particular, at the lowest order, the 3×3 light neutrino mass matrix can be expressed as

$$M_{\text{light}} = M_D M_N^{-1} M_D^T, \quad \text{with} \quad M_N = \mu_X M_X^{-1} \mu_X^T. \tag{2.33}$$

One then defines Majorana neutrino fields as

$$n_i = \begin{pmatrix} \nu_i \\ \overline{\nu_i} \end{pmatrix}$$

$$\text{with} \quad \nu_i = (U_\nu)_{ik}\nu_{L,k} + (U_\nu)_{i(k+3)} N^c_k + (U_\nu)_{i(k+6)} X_k, \tag{2.34}$$

where $i = 1, \ldots, 9$, $\quad k = 1, 2, 3$, and

$$\overline{\nu_i} = i\sigma_2 \nu^*_i. \tag{2.35}$$

The neutrino spectrum should contain three light active neutrinos n_i ($i = 1, 2, 3$) with masses of order eV and six heavy neutrinos n_I, $I = 4, \ldots, 9$. Their masses can be of order TeV. The diagonalization process can lead to negative mass eigenvalues, m_{n_x}, which in the version of the code for the CP-violating NMSSM we make positive by multiplying the corresponding x_{th} rotation matrix row with the imaginary unit i. So in our convention, the neutrino masses are all positive. In principle, one gives arbitrary inputs for M_D, μ_X, M_X and then obtains the corresponding neutrino masses and their rotation matrix. However, the obtained masses and mixing angles must satisfy the experimental data of the three active neutrinos. The chance to get parameter points passing these constraints starting from arbitrary input values is very low. A way out of this technical difficulty is to use a parameterization of M_D in terms of μ_X, M_X and the light neutrino masses and mixing angles. We follow the Casas–Ibarra parameterization [39], that makes use of the leading order relation for the light neutrino mass matrix

$$U^*_{\text{PMNS}} M_{\text{light}} U^\dagger_{\text{PMNS}} = m_\nu, \tag{2.36}$$

with

$$m_\nu = \text{diag}(m_{\nu_1}, m_{\nu_2}, m_{\nu_3}). \tag{2.37}$$

Using the expression of M_{light} given in (2.33) one then gets

$$M_D = U^T_{\text{PMNS}} \sqrt{m_\nu} R \sqrt{\mathcal{M}_N} V, \tag{2.38}$$

where

$$\mathcal{M}_N = \text{diag}(M_{N_1}, M_{N_2}, M_{N_3}). \tag{2.39}$$

The Pontecorvo–Maki–Nakagawa–Sakata (PMNS) matrix U_{PMNS} and the active neutrino masses m_{ν_i} (i = 1, 2, 3) are input values based on the available experimental data, while $M_{N_1}, M_{N_2}, M_{N_3}$ are the positive roots of M_N and V is a unitary matrix diagonalizing M_N as

$$\text{diag}(M_{N_1}, M_{N_2}, M_{N_3}) = V^* M_N V^\dagger, \tag{2.40}$$

and R is a complex orthogonal matrix that can be written in terms of three complex angles θ_i (i = 1, 2, 3)

$$R = \begin{pmatrix} c_2 s_3 & -c_1 s_3 - s_1 s_2 c_3 & s_1 s_3 - c_1 s_2 c_3 \\ c_2 s_3 & c_1 c_3 - s_1 s_2 s_3 & -s_1 c_3 - c_1 s_2 s_3 \\ s_2 & s_1 c_2 & c_1 c_2 \end{pmatrix}, \tag{2.41}$$

with $c_i = \cos\theta_i$, $s_i = \sin\theta_i$. In this study we set the three angles $\theta_{1,2,3}$ to be real. Using this Casas–Ibarra parameterization, the light neutrino masses denoted m_{n_i} $(i = 1, 2, 3)$ in (2.32) are approximately the input neutrino masses m_{ν_i} in (2.36). If the relative difference, defined as the maximum of $|(m_{n_i} - m_{\nu_i})/m_{\nu_i}|$ $(i = 1, 2, 3)$, is more than one percent, the code will print out a warning about the breakdown of the Casas–Ibarra parameterization.

With the introduction of the new superfields, the sneutrino sector is also changed. To incorporate CP violation, each sneutrino field is separated into its CP-even and CP-odd components as

$$\tilde{\nu} = \frac{1}{\sqrt{2}}(\tilde{\nu}_+ + i\tilde{\nu}_-) \tag{2.42}$$

$$\tilde{N}^* = \frac{1}{\sqrt{2}}\left(\tilde{N}_+ + i\tilde{N}_-\right) \tag{2.43}$$

$$\tilde{X} = \frac{1}{\sqrt{2}}\left(\tilde{X}_+ + i\tilde{X}_-\right). \tag{2.44}$$

The mass term in the basis $\psi = (\tilde{\nu}_+, \tilde{N}_+, \tilde{X}_+, \tilde{\nu}_-, \tilde{N}_-, \tilde{X}_-)^T$ (generation indices are suppressed) is given by

$$\mathcal{L} = \frac{1}{2}\psi^T M_{\tilde{\nu}} \psi, \tag{2.45}$$

where the mass matrix $M_{\tilde{\nu}}$ is an 18×18 symmetric matrix that can be found in Appendix B. An orthogonal matrix $U_{\tilde{\nu}}$ can be used to find the masses of the sneutrinos as follows,

$$\text{diag}\left(m^2_{\tilde{n}_1}, \ldots, m^2_{\tilde{n}_{18}}\right) = U_{\tilde{\nu}} M_{\tilde{\nu}} U_{\tilde{\nu}}{}^T, \tag{2.46}$$

where their mass values are ordered as $m^2_{\tilde{n}_1} \leq \cdots \leq m^2_{\tilde{n}_{18}}$.

3 Calculation of the neutral Higgs boson masses and mixings

In this section, we describe in detail our computation of the complete one-loop contribution to the loop-corrected neutral Higgs boson masses including the full momentum dependence and give a detailed description of the renormalization procedure. We apply dimensional reduction (DRED) [40,41] to regularize the UV-divergences, which has been proven to conserve SUSY at one-loop order. We have used several programs to compute the one-loop self-energies. To generate the Feynman diagrams and self-energies we use `FeynArts` [42,43] together with a model file created by `SARAH` [44–47]. The output self-energies were further processed using `FeynCalc` [48,49] for the simplification of the Dirac matrices and for the tensor reduction. The one-loop one- and two-point integrals were evaluated with a modified loop library of `NMSSMCALC` [50], in particular we used quadruple precision and complex external momentum squared for the two-point integrals to increase the convergence and stability of the code.[4] The new model and the calculation of the loop-corrected Higgs boson masses and mixings have been implemented in the code, called `NMSSMCALC-nuSS`. The code can be downloaded from the url:

https://www.itp.kit.edu/~maggie/NMSSMCALC-nuSS/

3.1 Loop-corrected Higgs boson masses and mixings

The loop-corrected Higgs boson masses can be obtained from the real parts of the complex mass eigenvalues of the 5×5 Higgs mass matrix with its elements

$$\mathcal{M}_{h_i h_j} = m^2_{h_i}\delta_{h_i h_j} - \hat{\Sigma}_{h_i h_j}(p^2), \quad i, j = 1, \ldots, 5, \tag{3.47}$$

where $\hat{\Sigma}_{h_i h_j}(p^2)$ is the renormalized self-energy of the transition $h_i \to h_j$ at external momentum squared p^2. We do not include the contributions due to the transitions $h_i \to G/Z$, since their contributions are negligible for light Higgs bosons. For extremely heavy Higgs bosons, they can have some effect as shown in [51].

The renormalized Higgs self-energies at one-loop level can be written in terms of the unrenormalized self-energies $\Sigma_{h_i h_j}(p^2)$ and the counterterms as

$$\begin{aligned} \hat{\Sigma}_{h_i h_j}(p^2) = \Sigma_{h_i h_j}(p^2) &+ \frac{1}{2}p^2\left[\mathcal{R}\left(\delta Z^\dagger_{hh} + \delta Z_{hh}\right)\mathcal{R}^T\right]_{ij} \\ &- \frac{1}{2}\left[\mathcal{R}\left(\delta Z^\dagger_{hh} M_{hh} + M_{hh}\delta Z_{hh}\right)\mathcal{R}^T\right]_{ij} \\ &- \left[\mathcal{R}\delta M_{hh}(\mathcal{R})^T\right]_{ij}. \end{aligned} \tag{3.48}$$

where the Higgs mass counterterm matrix is denoted by δM_{hh} and the wave-function renormalization constant matrix by δZ_{hh} in the basis (h_d, h_u, h_s, a, a_s). In Fig. 1, the one-loop Feynman diagrams contributing to the unrenormalized self-energies $\Sigma_{h_i h_j}(p^2)$ are shown. In the following sections, we will discuss the counterterms and renormalization conditions

[4] It is also possible to use double precision for the evaluation of the loop-corrected Higgs boson masses. This can be set in the makefile. However, for some parameter points, the convergence of the iterative method is not good compared to the usage of quadruple precision. This does not happen in the NMSSM without the seesaw mechanism.

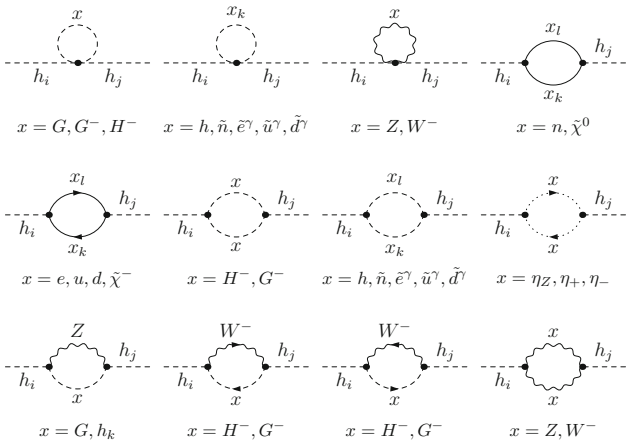

Fig. 1 Generic Feynman diagrams contributing to the one-loop neutral Higgs self-energies. The indices k, l take several sets of values depending on the fields that they go with: $k, l = 1, \ldots, 5$ for $x = h, \tilde{\chi}^0$, $k, l = 1, \ldots, 3$ for $x = e, u, d, \tilde{e}, \tilde{u}, \tilde{d}$, $k, l = 1, \ldots, 18$ for $x = \tilde{n}$ and $k, l = 1, \ldots, 9$ for $x = n$. The index γ denotes the left- and right-handed scalars. Color indices for the quarks and squarks are suppressed

in detail. We furthermore include the dominant two-loop corrections of order $\mathcal{O}(\alpha_s\alpha_t)$ [52] and $\mathcal{O}(\alpha_t^2)$ [33], which are available both for the real and for the complex NMSSM, to increase the precision for the phenomenological analysis presented in Sect. 5.

For the diagonalization of the loop-corrected mass matrix we apply the iterative method presented in [33,52–54].[5] For the loop-corrected n-th Higgs boson mass in the first iteration, the external momentum squared is set equal to the tree-level Higgs boson mass, $p^2 = m_{h_n}^2$. The obtained matrix is then diagonalized, yielding the n-th diagonal element. This value is then used as input momentum squared for the new iteration. The process is repeated until the change in p^2 between two consecutive iterations is less than 10^{-9}. The n-th loop-corrected mass squared $M_{h_n}^2$ is then defined as the real part of the last iterative n-th diagonal element.[6] The algorithm is repeated for all neutral Higgs boson masses. The loop-corrected masses are then sorted in ascending order, $M_{h_1} \leq M_{h_2} \leq M_{h_3} \leq M_{h_4} \leq M_{h_5}$. These loop-corrected masses obtained by the iterative method will be the outputs used in the decay width calculations and in the phenomenological study, if not stated otherwise.

[5] While this method includes contributions beyond the fixed-order renormalized self-energies, it can give rise to the gauge-parameter dependence of the loop-corrected masses due to the incomplete higher-order terms as studied in [35,51,55].

[6] We use capital M to denote loop-corrected masses in contrast to m for tree-level masses. For masses that are renormalized on-shell ($M_{H^\pm}, M_Z, M_W$, *cf.* Sect. 3.2.3) where the distinction need not be made, we use capital M as well.

We now define the loop-corrected mixing matrix that will be used to compute the effective couplings of the Higgs bosons with gauge bosons, fermions and among themselves. We define the loop-corrected mixing matrix R^0 to be the rotation of the loop-corrected mass matrix in the approximation of vanishing external momentum,

$$\begin{aligned}&\mathrm{diag}(M_{0,H_1}^2, M_{0,H_2}^2, M_{0,H_3}^2, M_{0,H_4}^2, M_{0,H_5}^2)\\ &\quad = R^0 \mathcal{M}_{hh}(0)(R^0)^T. \end{aligned} \tag{3.49}$$

The corresponding loop-corrected mass eigenvalues are denoted by an index 0 and sorted in ascending order, $M_{0,H_1} \leq M_{0,H_2} \leq M_{0,H_3} \leq M_{0,H_4} \leq M_{0,H_5}$. In this approximation, the mixing matrix R^0 is unitary but does not capture the proper OS properties of the external loop-corrected states as momentum-dependent effects are neglected. Using these thus defined mixing matrix elements, we obtain the Higgs effective couplings. Following the strategy presented in the NMSSMCALC [50], these Higgs effective couplings will be used to compute the Higgs decay widths, taking into account also higher-order QCD corrections when available.

3.2 Counterterms of the Higgs sector

Closely following the renormalization procedure at one-loop level described in [53,54], we choose the following set of quantities as our independent input,

$$\begin{aligned}&\big(t_{h_d}, t_{h_u}, t_{h_s}, t_{a_d}, t_{a_s}, e, M_W, M_Z, M_{H^\pm},\\ &\quad \tan\beta, v_s, |\lambda|, |\kappa|, \ \mathrm{Re}A_\kappa, \varphi_\lambda, \varphi_\kappa, \varphi_u, \varphi_s\big), \end{aligned} \tag{3.50}$$

where the five soft SUSY breaking parameters $\tilde{m}_{H_d}^2, \tilde{m}_{H_u}^2$, $\tilde{m}_S^2$, $\mathrm{Re}A_\lambda$, $\mathrm{Re}A_\kappa$ have been replaced by the five independent tadpoles $t_{h_d}, t_{h_u}, t_{h_s}, t_{a_d}, t_{a_s}$ which vanish at tree level. The complex phases $\varphi_\lambda, \varphi_\kappa, \varphi_u, \varphi_s$ do not need to be renormalized at one-loop level. The remaining input parameters are replaced by the sum of the corresponding renormalized parameters and their counterterm as

$$t_\phi \to t_\phi + \delta t_\phi \text{ with } \phi = (h_d, h_u, h_s, a_d, a_s) \tag{3.51}$$
$$M_{H^\pm}^2 \to M_{H^\pm}^2 + \delta M_{H^\pm}^2 \tag{3.52}$$
$$M_W^2 \to M_W^2 + \delta M_W^2 \tag{3.53}$$
$$M_Z^2 \to M_Z^2 + \delta M_Z^2 \tag{3.54}$$
$$e \to e(1 + \delta Z_e) \tag{3.55}$$
$$\tan\beta \to \tan\beta + \delta\tan\beta \tag{3.56}$$
$$v_s \to v_s + \delta v_s \tag{3.57}$$
$$|\lambda| \to |\lambda| + \delta|\lambda| \tag{3.58}$$
$$|\kappa| \to |\kappa| + \delta|\kappa| \tag{3.59}$$
$$\mathrm{Re}A_\kappa \to \mathrm{Re}A_\kappa + \delta\,\mathrm{Re}A_\kappa \tag{3.60}$$

The neutral Higgs boson counterterm matrix δM_{hh} in (3.48) can be written in terms of the counterterms of the input parameters. The analytical expression of δM_{hh} in terms of these counterterms can be found in Appendix C. In order to determine the counterterms, we need renormalization conditions. In this study, we use a mixture of the $\overline{\text{DR}}$and the OS scheme specified as

$$\underbrace{t_{h_d}, t_{h_u}, t_{h_s}, t_{a_d}, t_{a_s}, e, M_W, M_Z, M_{H^\pm}}_{\text{OS scheme}},$$
$$\underbrace{\tan\beta, v_s, |\lambda|, |\kappa|, \text{Re}A_\kappa}_{\overline{\text{DR}}\text{scheme}}. \tag{3.61}$$

In our code, there is also the possibility to chose $\text{Re}A_\lambda$ to be the input parameter instead of the charged Higgs mass. In this case $\Re A_\lambda$ is renormalized in the $\overline{\text{DR}}$scheme, while $M_{H^\pm}$ is computed at the same order as the one of the neutral Higgs boson masses.

The neutral Higgs wave function renormalization constants are introduced for the neutral components of both doublets and the singlet as

$$H_d \to \left(1+\frac{1}{2}\delta Z_{H_d}\right) H_d\,, \quad H_u \to \left(1+\frac{1}{2}\delta Z_{H_u}\right) H_u,$$
$$S \to \left(1+\frac{1}{2}\delta Z_S\right) S. \tag{3.62}$$

Hence the wave-function renormalization constant matrix introduced in (3.48) in the basis $\phi = (h_d, h_u, h_s, a, a_s)^T$ is given by

$$\phi \to \left(1+\frac{1}{2}\delta Z_{hh}\right)\phi, \tag{3.63}$$
$$\delta Z_{hh} = \text{diag}\left(\delta Z_{H_d}, \delta Z_{H_u}, \delta Z_S, s_\beta^2\delta Z_{H_d} + c_\beta^2\delta Z_{H_u}, \delta Z_S\right). \tag{3.64}$$

3.2.1 The neutral wave function renormalization constants

We use the $\overline{\text{DR}}$scheme to define the Higgs wave function renormalization constants.[7] The $\overline{\text{DR}}$scheme requires that the divergent part of the first derivative of the renormalized self-energies with respect to the momentum squared vanishes,

$$\widetilde{\text{Re}}\,\frac{\partial\hat{\Sigma}_{h_ih_j}(p^2)}{\partial p^2}\bigg|_{\text{div}} = 0, \quad \forall i,j = 1,\ldots,5, \tag{3.65}$$

where the notation $\widetilde{\text{Re}}$ means that only the real part of the loop integral is taken, and the superscript 'div' denotes the divergent part. This equation should hold for any external momentum. In practice we chose $p^2 = 0$. This renormalization condition leads to the equation

$$\delta Z_{h_ih_i} = -\left[\mathcal{R}^T\widetilde{\text{Re}}\,\frac{\partial\Sigma_{hh}}{\partial p^2}\bigg|_{\text{div}}\mathcal{R}\right]_{ii}, \tag{3.66}$$

which is real by definition and the off-diagonal elements vanish. Since δZ_{hh} contains only three unknown variables $\delta Z_{H_u}, \delta Z_{H_d}$ and δZ_S, one needs a set of three independent equations. Any chosen set must give the same solution due to the $SU(2)_L$ symmetry.

3.2.2 Tadpole renormalization

The tadpole counterterms are defined such that the minima of the Higgs potential do not change at higher order. The tadpole counterterms hence have to cancel any contribution from the diagrams at one-loop level leading to the renormalization conditions

$$\delta t_\phi = t_\phi, \phi = h_d, h_u, h_s, a_d, a_s, \tag{3.67}$$

with the one-loop tadpole diagrams contributing to t_ϕ depicted in Fig. 2.

3.2.3 Renormalization of $M_W, M_Z, M_{H^\pm}$

For the masses M_W, M_Z of the massive gauge bosons as well as $M_{H^\pm}$ of the charged Higgs boson we apply OS renormalization by requiring that the pole of the corresponding two-point correlation function at one-loop level occurs at the value of the input mass. In particular, the mass counterterms are given by the unrenormalized self-energies as

$$\delta M^2_{H^\pm} = \widetilde{\text{Re}}\Sigma_{H^+H^-}(M^2_{H^\pm}), \tag{3.68}$$
$$\delta M^2_W = \widetilde{\text{Re}}\Sigma^T_{WW}(M^2_W), \tag{3.69}$$
$$\delta M^2_Z = \widetilde{\text{Re}}\Sigma^T_{ZZ}(M^2_Z), \tag{3.70}$$

where the superscript T denotes the transverse parts of the respective self-energies. The wave function renormalization constants $\delta Z_{H^+H^-}$ for the charged Higgs boson, $\delta Z_{H^+G^-}$, $\delta Z_{H^+W^-}$ for the $H^+ - G^+/W^+$ mixings, $\delta Z_{W^+W^-}$ for the W boson, $\delta Z_{Z^+Z^-}$ for the Z boson and $\delta Z_{ZG}, \delta Z_{Z\gamma}$ for the $Z - G/\gamma$ mixings are all renormalized in the OS scheme, so that there is no additional contribution to Eqs. (3.68)–(3.70).

[7] While this renormalization is simple in practice, corrections arising from $\hat{\Sigma}_{h_ih_i}(\partial\hat{\Sigma}_{h_ih_i}(p^2)/\partial p^2)$ and from $\hat{\Sigma}_{h_ih_j}\hat{\Sigma}_{h_jh_i}/(m^2_{h_i} - m^2_{h_j})$ enter the loop-corrected masses, which are of higher order compared to the fixed order correction included in $\hat{\Sigma}_{h_ih_j}$. It is also possible to choose the OS scheme for the wave function renormalization constants, so that $(\partial\hat{\Sigma}_{h_ih_j}(p^2)/\partial p^2)$ and $\hat{\Sigma}_{h_ih_j}$ vanish at the tree-level Higgs masses. This can be done in the case where $m^2_{h_i}, m^2_{h_j}$ are very different in magnitude so that mixing effects can be expected to be small. In the other cases where the mixing terms are significant, by using the $\overline{\text{DR}}$scheme they are absorbed into the loop-corrected masses.

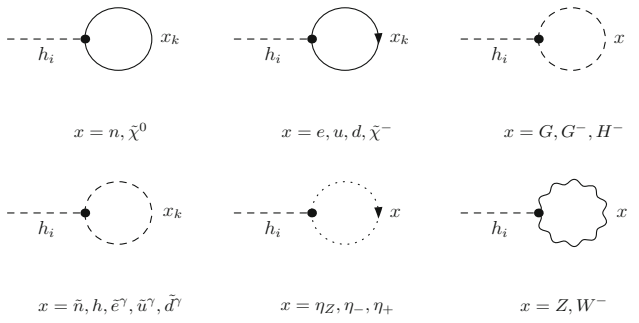

Fig. 2 Generic Feynman diagrams contributing to the one-loop tadpole counterterms. The index k is given by $k = 1, \ldots, 18$ for $x = \tilde{n}$, $k = 1, \ldots, 5$ for $x = h, \chi^0$, $k = 1, \ldots, 9$ for $x = n$ and $k = 1, \ldots, 3$ for $x = e, u, d, \tilde{e}, \tilde{u}, \tilde{d}$. The index γ denotes the left- and right-handed scalars. Color indices for the quarks and squarks are suppressed

3.2.4 Renormalization of the electric charge

The electric charge is renormalized in the OS scheme [56,57]. We take, however, the fine structure constant at the Z boson mass, $\alpha(M_Z^2)$, as input so that the counterterm is given by

$$\delta Z_e = \frac{1}{2}\left.\frac{\partial \Sigma^T_{\gamma\gamma}(k^2)}{\partial k^2}\right|_{k^2=0} + \frac{s_W}{c_W}\frac{\Sigma^T_{\gamma Z}(0)}{M_Z^2} - \frac{1}{2}\Delta\alpha(M_Z), \tag{3.71}$$

$$\Delta\alpha(M_Z) = \left.\frac{\partial \Sigma^{\text{light},T}_{\gamma\gamma}(k^2)}{\partial k^2}\right|_{k^2=0} - \frac{\widetilde{\text{Re}}\Sigma^{\text{light},T}_{\gamma\gamma}(M_Z^2)}{M_Z^2}, \tag{3.72}$$

where the photon self-energy $\Sigma^{\text{light},T}_{\gamma\gamma}$ includes only the light SM fermion (f with $m_f < m_t$) contributions.

3.2.5 Renormalization of $\tan\beta$

The ratio of the two vacuum expectation values, $\tan\beta$, is renormalized in the $\overline{\text{DR}}$scheme with the counterterm given by [58–60],

$$\delta\tan\beta = \frac{1}{2}\tan\beta\left(\delta Z_{H_u} - \delta Z_{H_d}\right)\Big|_{\text{div}}. \tag{3.73}$$

3.2.6 Renormalization of the remaining $\overline{DR}$ *quantities*

The renormalization of the remaining $\overline{\text{DR}}$quantities, δv_S, $\delta|\lambda|$, $\delta|\kappa|$, $\delta\text{Re}A_k$ is defined such that

$$\hat{\Sigma}_{h_i h_j}\Big|_{\text{div}} = 0. \tag{3.74}$$

This system has more equations than the number of unknown counterterms. We need only four independent equations to solve for the four counterterms. Any set of four chosen equations resulted in the same values for the counterterms, confirming that the renormalization procedure works. The resulting counterterms are checked numerically against the ones extracted from the one-loop beta-functions and anomalous dimensions obtained from the package `SARAH` [44–47]. The differences between our computed counterterms and `SARAH`'s are less than one per-mille.

4 Constraints

In this section, we discuss all constraints that have been taken into account in our present study. Since we concentrate on the effects of the loop corrections of the extended (s)neutrino sector on the loop-corrected Higgs masses and their mixing, we consider here only the most relevant constraints from the Higgs data, the active light neutrino oscillations, the electroweak precision observables, and the lepton flavor-violating radiative decays $l_1 \to l_2 + \gamma$.

4.1 Higgs data

Our model, which contains five neutral and two charged Higgs bosons, must satisfy the experimental results on the 125 GeV Higgs boson and the experimental constraints on new scalars. For a parameter point, we will calculate the Higgs boson masses including the available two-loop corrections at $\mathcal{O}\left(\alpha_t\alpha_s + \alpha_t^2\right)$ described in Sect. 3 and the Higgs decay widths and branching ratios including the state-of-the-art higher-order QCD corrections which we take from the code `NMSSMCALC` [50]. To check if a parameter point passes all the exclusion limits from searches at LEP, Tevatron and LHC we make use of the code `HiggsBounds-5` [61]. We provide the Higgs spectrum, decay widths, and the effective couplings as required by `HiggsBounds` in an SLHA file [62]. If the parameter point is allowed by `HiggsBounds`, it then will be checked against the 125 GeV Higgs boson data by using the code `HiggsSignals` [63]. We allow the uncertainty of the SM-like Higgs boson mass to be 3 GeV which means that at least one Higgs boson must have a mass in the range [122, 128] GeV. For the experimental data set, we use the "latestresults" option. Using our input parameters, `HiggsSignals` computes the χ^2 from 107 observables including the signal strength peak, simplified template cross sections, the LHC Run-1 signal rates, and Higgs masses. We allow the total χ^2 to vary within 2σ from the total χ^2 obtained from the SM Higgs boson. In `HiggsSignals-2.5.1`, the SM χ^2 is 84.44 and the 2σ for two degrees of freedom corresponds to a 6.18 χ^2 difference. Therefore the NMSSM χ^2 is allowed in the range [78.26, 90.62].

4.2 The active light neutrino data

In our neutrino sector, there are three light neutrinos which correspond to the three types of neutrinos observed in experiments. As discussed in Sect. 2, for the neutrino sector, we use the Casas–Ibarra parameterization. This means that we need three light mass values $m_{\nu_i}, i = 1, 2, 3$, three angles and one complex phase of the PMNS matrix, three complex angles of the orthogonal matrix R, defined in Eq. (2.41), together with the matrices μ_X and M_X to compute the mass matrix M_D specified in (2.38). The obtained M_D will be used to compute the neutrino Yukawa couplings y_ν and the neutrino mass matrix in (2.30). We then diagonalize this mass matrix using quadruple precision. The obtained mass eigenvalues m_{n_j} $(j = 1, \ldots, 9)$ are the neutrino mass eigenvalues. From the 9×9 neutrino mixing matrix we take the 3×3 block which describes the mixing between the three light neutrinos and define

$$N_{ij} = U^{\nu}_{ij}, \quad i, j = 1, 2, 3. \tag{4.75}$$

The N matrix is not unitary and can be written as

$$N = (I - \eta) U_{\text{PMNS}}. \tag{4.76}$$

We require that our input parameters, m_{ν_i}, $i = 1, 2, 3$, and U_{PMNS}, satisfy the active light neutrino data. We take the best fit points and the 3σ ranges from the global fit, NuFIT 5.0 [64]. For convenience, we list here the 3σ ranges for the mass differences and the mixing angles that are obtained from the combined analysis including the latest neutrino oscillation data presented at the "Neutrino2020" conference with the Super-Kamiokande atmospheric neutrino data. As usual, we define

$$\Delta m^2_{ij} = m^2_{\nu_i} - m^2_{\nu_j},$$
$$U_{\text{PMNS}} = \begin{pmatrix} c_{12}c_{13} & s_{12}c_{13} & s_{13}e^{-i\delta_{CP}} \\ -s_{12}c_{23} - c_{12}s_{23}s_{13}e^{i\delta_{CP}} & c_{12}c_{23} - s_{12}s_{23}s_{13}e^{i\delta_{CP}} & s_{23}c_{13} \\ s_{12}s_{23} - c_{12}c_{23}s_{13}e^{i\delta_{CP}} & -c_{12}s_{23} - s_{12}c_{23}s_{13}e^{i\delta_{CP}} & c_{23}c_{13} \end{pmatrix}, \tag{4.77}$$

where the short-hand notation $c_{ij} = \cos\theta_{ij}$ and $s_{ij} = \sin\theta_{ij}$ has been used. We request that

$$\Delta m^2_{21} \in [6.82, 8.04] \times 10^{-5}\ \text{eV}^2, \quad s^2_{12} \in [0.269, 0.343], \tag{4.78}$$

and for the normal ordering

$$\begin{aligned} &\Delta m^2_{31} \in [2.435, 2.598] \times 10^{-3}\ \text{eV}^2, \\ &s^2_{23} \in [0.415, 0.616], \\ &s^2_{13} \in [0.02032, 0.02410], \quad \delta_{CP} \in [120, 369], \end{aligned} \tag{4.79}$$

and for the inverted ordering

$$\begin{aligned} &\Delta m^2_{23} \in [2.414, 2.581] \times 10^{-3}\ \text{eV}^2, \\ &s^2_{23} \in [0.419, 0.617], \\ &s^2_{13} \in [0.02052, 0.02428], \quad \delta_{CP} \in [193, 352]. \end{aligned} \tag{4.80}$$

In our analysis we use the constraint on the non-unitary N matrix that arises from a combined analysis of short and long-baseline neutrino oscillation data [65]. We use the three most stringent bounds at the 3σ CL expressed in a parameterization-independent way, in particular

$$\begin{aligned} 1 - \sum_{k=1}^{3} N_{ek} N^*_{ek} &< 0.07, \\ 1 - \sum_{k=1}^{3} N_{\mu k} N^*_{\mu k} &< 0.07, \\ \sum_{k=1}^{3} N_{ek} N^*_{\mu k} &< 0.03. \end{aligned} \tag{4.81}$$

This constraint will be denoted as non-unitary constraint in the numerical Sect. 5.2.

Furthermore, we use the Planck 2018 results for the upper limit of the sum of the three light neutrino masses,

$$\sum_{i=1}^{3} m_{\nu_i} < 0.12\,\text{eV}. \tag{4.82}$$

4.3 The oblique parameters

The presence of the supersymmetric particles, multiple Higgs boson states and sterile neutrinos affects the masses and decay properties of the electroweak bosons and the low-energy data. We use the three well-known gauge self-energy parameters S, T and U [66] at the one-loop level to describe the effects arising from new particles. Following [67], we also define the parameters S, T, U from the transverse part of the gauge boson self-energies as

$$\begin{aligned} T &= \frac{1}{\alpha}\left(\frac{\Pi^{\text{new}}_{WW}(0)}{M^2_W} - \frac{\Pi^{\text{new}}_{ZZ}(0)}{M^2_Z}\right), \\ S &= \frac{4s^2_W c^2_W}{\alpha}\left(\frac{\Pi^{\text{new}}_{ZZ}(M^2_Z) - \Pi^{\text{new}}_{ZZ}(0)}{M^2_Z}\right. \end{aligned} \tag{4.83}$$

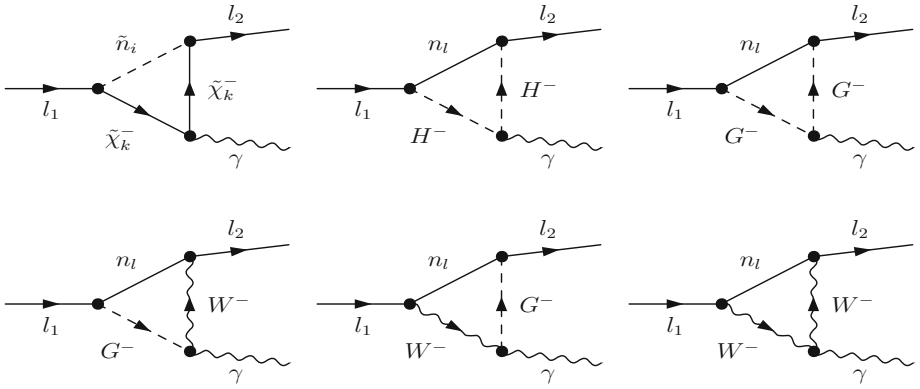

Fig. 3 Generic Feynman diagrams contributing to the charged lepton flavor-violating decays $l_1 \to l_2 + \gamma$. The ranges of the indices are $i = 1, \ldots, 18$, $k = 1, 2$ and $l = 1, \ldots, 9$

$$- \frac{c_W^2 - s_W^2}{s_W c_W} \frac{\Pi_{Z\gamma}^{\text{new}}(M_Z^2)}{M_Z^2} - \frac{\Pi_{\gamma\gamma}^{\text{new}}(M_Z^2)}{M_Z^2}\Bigg), \tag{4.84}$$

$$S + U = \frac{4 s_W^2}{\alpha}\Bigg(\frac{\Pi_{WW}^{\text{new}}(M_W^2) - \Pi_{WW}^{\text{new}}(0)}{M_W^2} - \frac{c_W}{s_W}\frac{\Pi_{Z\gamma}^{\text{new}}(M_Z^2)}{M_Z^2} - \frac{\Pi_{\gamma\gamma}^{\text{new}}(M_Z^2)}{M_Z^2}\Bigg), \tag{4.85}$$

where the fine structure constant α is given at the scale M_Z. The superscript "new" means that we have subtracted the SM contribution computed with a Higgs boson mass of 125 GeV so that only new physics contributions remain. Using data from physics at the Z pole, [67] has found the following best fit point and 1σ uncertainties for these parameters,

$$T = 0.03 \pm 0.12, \tag{4.86}$$

$$S = -0.01 \pm 0.10, \tag{4.87}$$

$$U = 0.02 \pm 0.11. \tag{4.88}$$

In our analysis, a valid parameter point satisfies constraints on new physics if the S, T, U values vary within the 1σ uncertainty ranges around the best fit point.

4.4 The radiative $l_1 \to l_2 + \gamma$ decays

We work in the NMSSM in which the soft SUSY breaking mass matrices $\tilde{m}_L^2, \tilde{m}_E^2$ and trilinear couplings A_e as well as the Yukawa couplings y_e are diagonal in any basis. In general, if off-diagonal elements of these matrices exist, they have large effects on charged lepton flavor-violating (LFV) processes which have been severely constrained [68]. Although in our setting these matrices are flavor conserving, the presence of the low-scale sterile neutrinos and mixings with active neutrinos can still induce large charged LFV processes. The most constraining LFV processes are the radiative decays $\tau \to \mu\gamma$, $\tau \to e\gamma$ and $\mu \to e\gamma$, which are calculated in this section. The corresponding experimental bounds at 90% confidence level [67] are

$$\text{BR}(\mu^- \to e^-\gamma) < 4.2 \times 10^{-13}, \tag{4.89}$$

$$\text{BR}(\tau^- \to e^-\gamma) < 3.3 \times 10^{-8}, \tag{4.90}$$

$$\text{BR}(\tau^- \to \mu^-\gamma) < 4.4 \times 10^{-8}. \tag{4.91}$$

These processes have been widely studied in the literature for non-supersymmetric models and the MSSM using the exact diagonalization of the mass matrices or using the mass insertion approximation, for a review see [69] and references therein. In our calculation we use the exact diagonalization of the relevant (s)neutrino mass matrices. We have used the model file obtained from `SARAH` to generate one-loop Feynman diagrams and amplitudes using `FeynArts`, and further simplified the amplitudes with the help of the package `FeynCalc`. The one-loop Feynman diagrams contributing to the decay processes

$$l_1(p) \to l_2(p-q) + \gamma(q) \tag{4.92}$$

are depicted in Fig. 3. The amplitude of this process is given by

$$\mathcal{A} = i\epsilon_\mu^*(q)\mathcal{M}^\mu, \tag{4.93}$$

where ϵ_μ denotes the polarization vector of the external photon. Using gauge invariance, $q_\mu \mathcal{M}^\mu = 0$, we can prove that $\mathcal{M}^\mu$ must take the form

$$\mathcal{M}^\mu = \bar{u}_2 \sigma^{\mu\nu} q_\nu \left(F_L P_L + F_R P_R\right) u_1, \tag{4.94}$$

where $\sigma^{\mu\nu} = i/2\left[\gamma^\mu, \gamma^\nu\right]$, $P_{L/R} = (1 \mp \gamma_5)/2$ and $F_{L/R}$ are left- and right-handed form factors. The partial width is then given by

$$\Gamma(l_1 \to l_2\gamma) = \frac{m_1^3}{16\pi}\left(|F_L|^2 + |F_R|^2\right), \tag{4.95}$$

where m_1 is the mass of l_1 and we have neglected the mass of l_2 since $m_2 \ll m_1$ for the processes considered here. Following the common procedure presented in [70], the branching ratios of the decays $l_1 \to l_2\gamma$ can be written in terms of the branching ratios of $l_1 \to l_2\bar{\nu}_2\nu_1$ which are experimentally

measured. In the NMSSM, the tree-level decay width for the decays $l_1 \to l_2 \bar{\nu}_2 \nu_1$ is the same as that of the SM, i.e.

$$\Gamma(l_1 \to l_2 \bar{\nu}_2 \nu_1) = \frac{G_F^2 m_1^5}{192\pi^3}; \tag{4.96}$$

therefore,

$$\begin{aligned} &\mathrm{BR}(l_1 \to l_2 \gamma) \\ &= \frac{12\pi^2}{G_F^2 m_1^2} \left(|F_L|^2 + |F_R|^2 \right) \mathrm{BR}(l_1 \to l_2 \bar{\nu}_2 \nu_1). \end{aligned} \tag{4.97}$$

We use the following numerical values taken from [68] for the branching ratios,

$$\begin{aligned} &\mathrm{BR}(\mu \to e \bar{\nu}_e \nu_\mu) = 1, \quad \mathrm{BR}(\tau \to e \bar{\nu}_e \nu_\tau) = 17.82\%, \\ &\mathrm{BR}(\tau \to \mu \bar{\nu}_\mu \nu_\tau) = 17.39\%. \end{aligned} \tag{4.98}$$

The contributions to the form factors in our model can be decomposed into three parts as

$$F_{L,R} = F_{L,R}^{W^\pm} + F_{L,R}^{H^\pm} + F_{L,R}^{\tilde{\chi}^\pm}, \tag{4.99}$$

where $F_{L,R}^{W^\pm}$, $F_{L,R}^{H^\pm}$ and $F_{L,R}^{\tilde{\chi}^\pm}$ denote the contributions from the one-loop diagrams with $W^\pm$ and charged Goldstone bosons, charged Higgs bosons and charginos, respectively, on the internal lines. Their explicit expressions are given in Appendix A. Since in the numerical analysis, all the $\overline{\mathrm{DR}}$input parameters are given at the SUSY scale, we do not consider contributions from the off-diagonal elements of $\tilde{m}_L^2$, $\tilde{m}_E^2$, A_e due to the renormalization group equations as discussed in [39].

It is also possible to keep the lepton masses of the external lines in the three-point loop integrals. However, we explicitly checked that the differences between the branching ratios obtained with the full lepton masses using `Mathematica` and the ones with zero lepton masses are below the per-mille level. The same result has been found in the Standard Model case [71]. We, therefore, use the zero lepton mass approximation implemented in the code `NMSSMCALC-nuSS` in the numerical analysis.

5 Numerical analysis

In this section we will discuss the numerical impact of the neutrino and sneutrino sectors on the loop-corrected neutral Higgs boson masses and on the charged lepton flavor-violating decays. We have performed a scan over the parameter space of our model to obtain parameter points that satisfy all our constrains mentioned in Sect. 4. We chose SM input parameters as [67,72]

$$\begin{aligned} &\alpha(M_Z) = 1/127.955, && \alpha_s^{\overline{\mathrm{MS}}}(M_Z) = 0.1181, \\ &M_Z = 91.1876\ \mathrm{GeV}, && M_W = 80.379\ \mathrm{GeV}, \\ &m_t = 172.74\ \mathrm{GeV}, && m_b^{\overline{\mathrm{MS}}}(m_b^{\overline{\mathrm{MS}}}) = 4.18\ \mathrm{GeV}, \\ &m_c = 1.274\ \mathrm{GeV}, && m_s = 95.0\ \mathrm{MeV}, \\ &m_u = 2.2\ \mathrm{MeV}, && m_d = 4.7\ \mathrm{MeV}, \\ &m_\tau = 1.77682\ \mathrm{GeV}, && m_\mu = 105.6584\ \mathrm{MeV}, \\ &m_e = 510.9989\ \mathrm{KeV}, && G_F = 1.16637 \cdot 10^{-5}\ \mathrm{GeV}^{-2}. \end{aligned} \tag{5.100}$$

The light neutrino inputs are in the normal ordering and according to the constraints in Sect. 4.2 are chosen randomly in the following ranges

$$\begin{aligned} &m_{\nu_1} \in [0, 2.98152 \times 10^{-11}]\ \mathrm{GeV}, \\ &m_{\nu_2} \in \left[\sqrt{m_{\nu_1}^2 + 6.82 \times 10^{-23}}, \right. \\ &\left. \sqrt{m_{\nu_1}^2 + 8.04 \times 10^{-23}} \right]\ \mathrm{GeV}, \\ &m_{\nu_3} \in \left[\sqrt{m_{\nu_1}^2 + 2.435 \times 10^{-21}}, \right. \\ &\left. \sqrt{m_{\nu_1}^2 + 2.598 \times 10^{-21}} \right]\ \mathrm{GeV}, \\ &\theta_{12} \in [\arcsin(\sqrt{0.269}), \arcsin(\sqrt{0.343})], \\ &\theta_{23} \in [\arcsin(\sqrt{0.415}), \arcsin(\sqrt{0.617})], \\ &\theta_{13} \in [\arcsin(\sqrt{0.02052}), \arcsin(\sqrt{0.02428})], \\ &\delta_{CP} \in [120, 369]. \end{aligned} \tag{5.101}$$

Following the convention of the SUSY Les Houches Accord (SLHA) format [62], the soft SUSY breaking masses and trilinear couplings are understood as $\overline{\mathrm{DR}}$ parameters at the scale

$$\mu_R = M_{\mathrm{SUSY}} = \sqrt{m_{\tilde{Q}_3} m_{\tilde{t}_R}}. \tag{5.102}$$

This is also the renormalization scale that we use in all of our computations of the higher-order corrections. In the Higgs sector we use per default the mixed $\overline{\mathrm{DR}}$-OS scheme specified in Sect. 3.2 and the OS charged Higgs boson mass as input parameters. Furthermore, we choose OS renormalization for the top/stop sector and include the two-loop corrections of order $\mathcal{O}(\alpha_s \alpha_t + \alpha_t^2)$ which are computed in [32,33] and are implemented in `NMSSMCALC`. We perform the scan in the framework of the CP-violating NMSSM where we chose the phase δ_{CP} in the neutrino sector as the only non-vanishing complex phase. All other SUSY parameters are assumed to be real and are varied in the ranges specified in Table 2.

The remaining parameters are fixed as follows

Table 2 Scan ranges for the random scan over the NMSSM parameter space

Parameter	Scan range
$M_{H^\pm}$	[0.6, 1] TeV
M_1, M_2	[0.5, 1] TeV
μ_{eff}	[0.2, 1] TeV
$m_{\tilde{Q}_3}, m_{\tilde{t}_R}$	[1, 3] TeV
$m_{\tilde{L}_3}, m_{\tilde{\tau}_R}$	[1, 3] TeV
A_t	[− 4, 4] TeV
$\Re A_\kappa$	[− 2, 2] TeV
$\tan\beta$	[1, 10]
λ	[0.0001, 0.7]
κ	[0.0001, 0.7]
$m_{\tilde{X}}$	[1, 3] TeV
$m_{\tilde{N}}$	[1, 3] TeV
A_ν	[− 2, 2] TeV
A_X	[− 2, 2] TeV
μ_X	[1, 100] TeV
B_{μ_X}	[1, 1000] GeV
λ_X	$[10^{-12}, 10^{-8}]$
$\theta_{1,2,3}$	$[0, 2\pi]$

$$M_3 = 1850\ \text{GeV}, \quad m_{\tilde{Q}_{1/2}} = m_{\tilde{L}_{1/2}} = m_{\tilde{x}_R} = 3\ \text{TeV}, \quad A_{b,\tau} = 2\ \text{TeV} \tag{5.103}$$

where $x = u, d, c, s, b, e, \mu$. To ensure perturbativity below the GUT scale [73] we omit points with

$$\kappa^2 + \lambda^2 > (0.7)^2, \tag{5.104}$$

and/or any element of the neutrino Yukawa matrix y_ν being larger than $\sqrt{4\pi}$. Note that in our numerical analysis we take the various input parameters of the (s)neutrino sector to be the same for all three generations.

5.1 Impact of the (s)neutrinos on the loop-corrected Higgs boson masses

For the investigation of the impact of the (s)neutrino contributions on the loop-corrected Higgs boson masses we choose a parameter point from our generated scan sample satisfying all the described constraints. We subsequently vary individual parameters of the neutrino and/or sneutrino sectors to analyze their impact on the loop-corrected Higgs boson masses. Our chosen parameter point is called `P1`. The light neutrino input parameters are set equal to their best-fit values together with a fixed value for the lightest neutrino mass, in particular,

$$\begin{aligned} m_{\nu_1} &= 10^{-11} & \theta_{12} &= \arcsin(\sqrt{0.297}), \\ m_{\nu_2} &= \sqrt{m_{\nu_1}^2 + 7.37 \times 10^{-23}}\ \text{GeV}, & \theta_{23} &= \arcsin(\sqrt{0.425}), \\ m_{\nu_3} &= \sqrt{m_{\nu_1}^2 + 2.525 \times 10^{-21}}\ \text{GeV} & \theta_{13} &= \arcsin(\sqrt{0.0215}), \\ \delta_{CP} &= 248.4^\circ. \end{aligned}$$

All other complex phases are set to zero and the remaining input parameters are given by

$$\begin{aligned} M_{H^\pm} &= 850\ \text{GeV}, & m_{\tilde{X}} &= 1\ \text{TeV}, \\ M_1 &= 660\ \text{GeV}, & m_{\tilde{N}} &= 1\ \text{TeV}, \\ M_2 &= 580\ \text{GeV}, & A_\nu &= 1.2\ \text{TeV}, \\ \mu_{\text{eff}} &= 208\ \text{GeV}, & A_X &= 1\ \text{TeV}, \\ m_{\tilde{Q}_3} &= 1300\ \text{GeV}, & \mu_X &= 40\ \text{TeV}, \\ m_{\tilde{t}_R} &= 1100\ \text{GeV}, & B_{\mu_X} &= 1\ \text{TeV}, \\ m_{\tilde{\tau}_R} &= 1900\ \text{GeV}, & \lambda_X &= 6.5 \times 10^{-10}, \\ A_t &= -1500\ \text{GeV}, & \theta_1 &= 2, \\ \text{Re}A_k &= -791\ \text{GeV}, & \theta_2 &= 3, \\ \tan\beta &= 4.4, & \theta_3 &= 4, \\ \lambda &= 0.30, & \kappa &= 0.30. \end{aligned} \tag{5.105}$$

In Table 3, we present the Higgs mass spectrum with and without inverse seesaw mechanism at tree-level, one-loop, two-loop $\mathcal{O}(\alpha_t\alpha_s)$ and two-loop $\mathcal{O}(\alpha_t\alpha_s + \alpha_t^2)$. The main components of the Higgs mass eigenstates are also shown in the last row. We have chosen the OS condition for the top/stop sector. In order to quantify the impact of the (s)neutrino contributions on the Higgs boson masses we define the relative correction Δ_i as

$$\Delta_i = \left| \frac{M_i - M_i^{\text{no}}}{M_i^{\text{no}}} \right| \tag{5.106}$$

where M_i is the loop-corrected mass of the Higgs boson i computed in the NMSSM with ISS and M_i^{no} the one in the NMSSM without ISS. Note that the NMSSM without ISS mechanism contains three massless neutrinos and three complex sneutrinos which do not mix with each other. The massless neutrinos do not interact with the Higgs bosons while the sneutrinos couple to the Higgs bosons through the D-terms with couplings proportional to g_1 and g_2. For this parameter point the second lightest Higgs boson is the h_u-like one and hence behaves SM-like. The h_s-like Higgs boson is the lightest one with a mass of 90 GeV. The h_d- and a-like states have masses of about 850 GeV while the a_s-like Higgs boson mass is about 700 GeV. Although we have a non-zero complex phase in the U_{PMNS} matrix, the mixing between CP-even and CP-odd states is negligible. The h_u-like Higgs boson mass is affected the most by the inclusion

Table 3 Parameter point P1: mass values in GeV and main components of the neutral Higgs bosons at tree-level, one-loop, two-loop $\mathcal{O}(\alpha_t\alpha_s)$ and two-loop $\mathcal{O}(\alpha_t\alpha_s+\alpha_t^2)$ obtained for the NMSSM without or with the inverse seesaw mechanism together with OS conditions in the top/stop sector

	h_1	h_2	h_3	h_4	h_5
Tree-level	84.96	85.38	705.10	847.86	850.00
One-loop					
Without ISS	90.31	129.77	700.63	847.76	849.95
With ISS	89.43	136.62	701.07	848.06	850.74
Two-loop $\mathcal{O}(\alpha_t\alpha_s)$					
Without ISS	90.21	114.69	700.65	847.77	849.88
With ISS	89.17	119.52	701.08	848.06	850.62
Two-loop $\mathcal{O}(\alpha_t\alpha_s+\alpha_t^2)$					
Without ISS	90.24	120.72	700.65	847.77	849.91
With ISS	89.28	126.37	701.08	848.06	850.67
Main component	h_s	h_u	a_s	a	h_d

of the ISS mechanism which raises M_{h_u} by about 7 GeV, 5 GeV and 5.6 GeV at one-loop level, $\mathcal{O}(\alpha_t\alpha_s)$ and $\mathcal{O}(\alpha_t^2)$, respectively. If we quantify this change by using the relative correction defined in (5.106) we see that Δ_{h_u} is about 5.3% at one-loop level, then decreases to 4.2% at $\mathcal{O}(\alpha_t\alpha_s)$ and reaches 4.7% at $\mathcal{O}(\alpha_t\alpha_s+\alpha_t^2)$. We remind the reader that we have used the iterative method to evaluate the loop-corrected Higgs boson masses. This means that we have mixed orders of perturbation theory. As common in supersymmetric theories, loop contributions from particles and their superpartners are opposite in sign. This is the case for the neutrinos and sneutrinos here as well. While the sneutrinos give positive contributions to the mass M_{h_u}, those of the neutrinos are negative. Soft-SUSY breaking terms together with electroweak symmetry breaking prohibit the cancellation between the two contributions. We will elaborate this further in the following by varying parameters related to the change of these two contributions. We finish our comments on Table 3 by remarking that the other Higgs boson masses are only slightly changed by the ISS for this particular point.

We continue by investigating the effects of the various neutrino parameters on the loop-corrected Higgs boson masses. From now on we present only the masses at two-loop $\mathcal{O}(\alpha_t\alpha_s+\alpha_t^2)$ which is the highest precision of our numerical code that includes the ISS.[8] In Fig. 4 we show the dependence of the loop-corrected Higgs boson masses on the coupling λ_X in the left panel and on the mass μ_X in the right panel and the dependence of the correction Δ defined in (5.106) in the lower panels. We remind the reader that both λ_X and μ_X appear in the neutrino mixing matrix as shown in (2.30) and (2.31). In the Casas–Ibarra parameterization which is used in our computation, both λ_X and μ_X enter the evaluation of the neutrino Dirac mass matrix M_D, see (2.38), therefore directly affect the neutrino Yukawa matrix $Y_\nu = \sqrt{2}M_D/(v_u e^{i\varphi_u})$ that can be written as

$$Y_\nu \propto \frac{m_\nu\sqrt{\mu_X}}{v_u\sqrt{\lambda_X}v_s}. \tag{5.107}$$

We denote the maximum element of the neutrino Yukawa matrix by $Y_\nu^{\max}$. We chose the range of variation for λ_X and μ_X such that $Y_\nu^{\max}$ is smaller than the perturbativity limit $\sqrt{4\pi}$ applied in our analysis. On the x-axis on top of each plot in Fig. 4, we see the variation of $Y_\nu^{\max}$ corresponding to the range of variation for λ_X and μ_X. For our chosen parameter point P1, the value of $Y_\nu^{\max}$ is equal to 1.15. As can be inferred from the plots, the impact from the (s)neutrino sector is less than 2.3% on M_{h_u} if $Y_\nu^{\max}$ is smaller than 0.85 (0.89) corresponding to $\lambda_X > 1.2\times10^{-9}$ ($\mu_X < 31$ TeV) in the left (right) plot. With increasing value of $Y_\nu^{\max}$ (λ_X becomes smaller or μ_X gets larger) the effect increases significantly. The relative correction Δ_{h_u} can even go up to 100% for $\lambda_X = 1.24\times10^{-10}$ ($Y_\nu^{\max} = 2.63$) or $\mu_X = 83$ TeV ($Y_\nu^{\max} = 2.39$). This makes us question the perturbativity limit of $\sqrt{4\pi}$ applied on $Y_\nu^{\max}$ at the SUSY scale. A more stringent constraint that demands $Y_\nu^{\max} < \sqrt{4\pi}$ up to the Planck scale may imply a much smaller value for $Y_\nu^{\max}$ at the SUSY scale. A recent study in [75] found that $Y_\nu^{\max} < 0.8$ at the TeV scale for the SM with inverse seesaw mechanism. We expect a similar value for the model in our study. The large value of μ_X results in large mass values for the sterile neutrinos and additional sneutrinos. One then has to worry about the validity of the fixed-order calculation used in the computation of the Higgs mass corrections. In order to understand the role of y_ν and μ_X, we present in Appendix D the approximate expressions for the additional contributions from the NMSSM with inverse seesaw mechanism after subtracting the usual NMSSM contributions to the renormalized h_u-like Higgs self-energy. Caution should be taken here when using these approximate formulae to reproduce the results. We have applied many conditions specified in the appendix to derive these approximate formulae. We have checked that the expression given in Eq. (D.166) can deviate by about 10% from the full one-loop (s)neutrino corrections with full momentum dependence and mixing between different neutral Higgs bosons. If the specified conditions are not satisfied, however, the deviation can be much larger and these approximations are not reliable. In (D.172), there is a term proportional to $\log\left(\frac{\mu_X}{\mu_R}\right)$ which causes large corrections if $\mu_X \gg \mu_R$. The question of what should be done to improve the precision and to reduce the theoretical uncertainty of the loop-corrected Higgs masses will be left for future study. In

[8] We very recently completed the two-loop contributions at $\mathcal{O}((\alpha_t+\alpha_\lambda+\alpha_\kappa)^2)$ [74]. They are included in NMSSMCALC and NMSSMCALCEW and will soon be included in NMSSMCALC-nuSS as well.

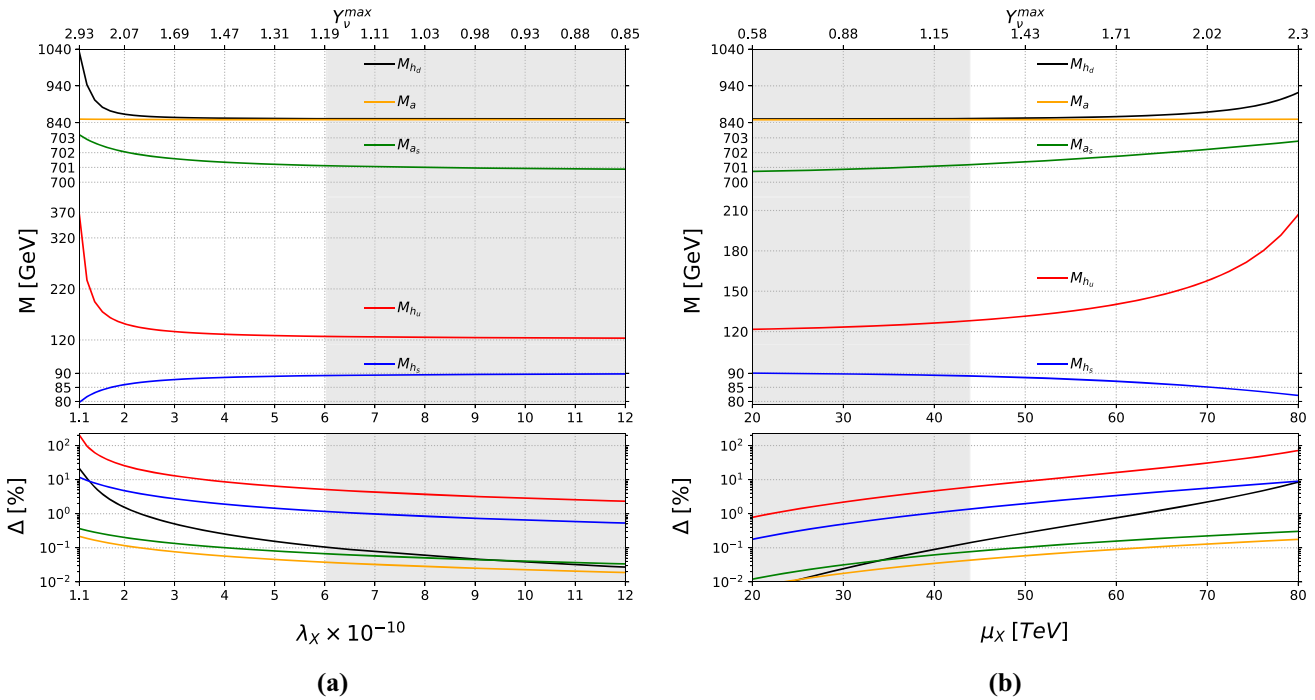

Fig. 4 Parameter point P1: The loop-corrected Higgs boson masses in GeV at order $\mathcal{O}\left(\alpha_t\alpha_s + \alpha_t^2\right)$ as function of the parameter λ_X (upper left) and of μ_X (upper right) The relative corrections Δ defined in (5.106) are shown in the lower panels. The five Higgs boson masses are denoted by their main components (h_u, h_d, h_s, a, a_s) corresponding to the five colors (red, black, blue, yellow, green). The gray area on the plots denotes the points satisfying our constraints. $Y_\nu^{\max}$ denotes the maximum element of the neutrino Yukawa matrix

this study we retain parameter points where $\log\left(\frac{\mu_X}{\mu_R}\right)$ is less than four. The question whether this logarithm is the main source of the large correction can be answered by choosing a much smaller value for μ_X, for example of $\mathcal{O}(\mu_R)$. We can still get a large value for Δ_{h_u}, as long as $Y_\nu^{\max}$ is large. In particular, for $\mu_X = 1500\,\text{GeV}$ and $\lambda_X = 1.8 \times 10^{-12}$, Δ_{h_u} is of order 5%. With a low mass spectrum of sterile neutrinos and sneutrinos one can get large branching ratios for the charged lepton flavor-violating processes $l_1 \to l_2 + \gamma$ that will be discussed in Sect. 5.2. The parameter point with $\mu_X = 1500\,\text{GeV}$ and $\lambda_X = 1.8 \times 10^{-12}$ does not pass the charged lepton flavor-violating constraint. The question arises whether $\Delta_{h_u} \sim 5\%$ with low μ_X can be realized for parameter points satisfying all our considered constraints. We can find such parameter points where M_D in (2.38) is almost a diagonal matrix. As a result, the decay widths of $l_1 \to l_2 + \gamma$ are close to zero, since they are proportional to off-diagonal components of y_ν. In such a case, it may be better to use, for example, the μ_X-parameterization [76] instead of the Casas–Ibarra parameterization. In the μ_X-parameterization, λ_X is not an input parameter but computed from the relations

$$M_X = \mu_X^T M_D^{-1} U_{\text{PMNS}}^* m_\nu U_{\text{PMNS}}^\dagger M_D^{T,-1} \mu_X,$$
$$M_X = \frac{v_s e^{i\varphi_s}}{\sqrt{2}}(\lambda_X + \lambda_X^T), \tag{5.108}$$

where y_ν is now an input parameter. One can easily choose y_ν to be the unit matrix, then with $\mu_X = 1500\,\text{GeV}$, one can get $\Delta_{h_u} \sim 5\%$.

From Fig. 4, we see that not only the h_u-like Higgs boson is strongly affected by large $Y_\nu^{\max}$ but also the h_d- and h_s-like states. While both the h_u- and h_d-like Higgs boson mass get positive corrections, the h_s-like Higgs boson mass receives negative corrections. On the left plot Δ_{h_d} can go up to 21% at $Y_\nu^{\max} = 2.93$ while Δ_{h_s} goes to 12%. Note that neutrinos interact with h_u interaction states through the interaction term $h_u \bar{\nu}_i (Y_\nu P_L + Y_\nu^\dagger P_R)\nu_j$ and with h_s through the interaction term $h_s \bar{\nu}_i (\lambda_X P_L + \lambda_X^\dagger P_R)\nu_j$ where λ_X is a very small number. Neutrinos do not interact with h_d, but sneutrino do interact through D-terms. For this particular parameter point, the dominantly h_d- and h_s-like Higgs mass eigenstates have a significant admixture of the h_u component. The impact of the neutrinos on the other Higgs bosons depends on their mixtures with h_u. The states a and a_s are less affected.

We now move on to the discussion of the dependence of the loop-corrected Higgs boson masses on the neutrino trilinear coupling parameter A_ν that affects only the sneutrino sector and leaves the neutrino sector unchanged. In Fig. 5 we vary the value of A_ν in the left plots and the complex phase of A_ν in the right plots. The color code and notation of the left plots are the same as in Fig. 4. In the right plot, we show only

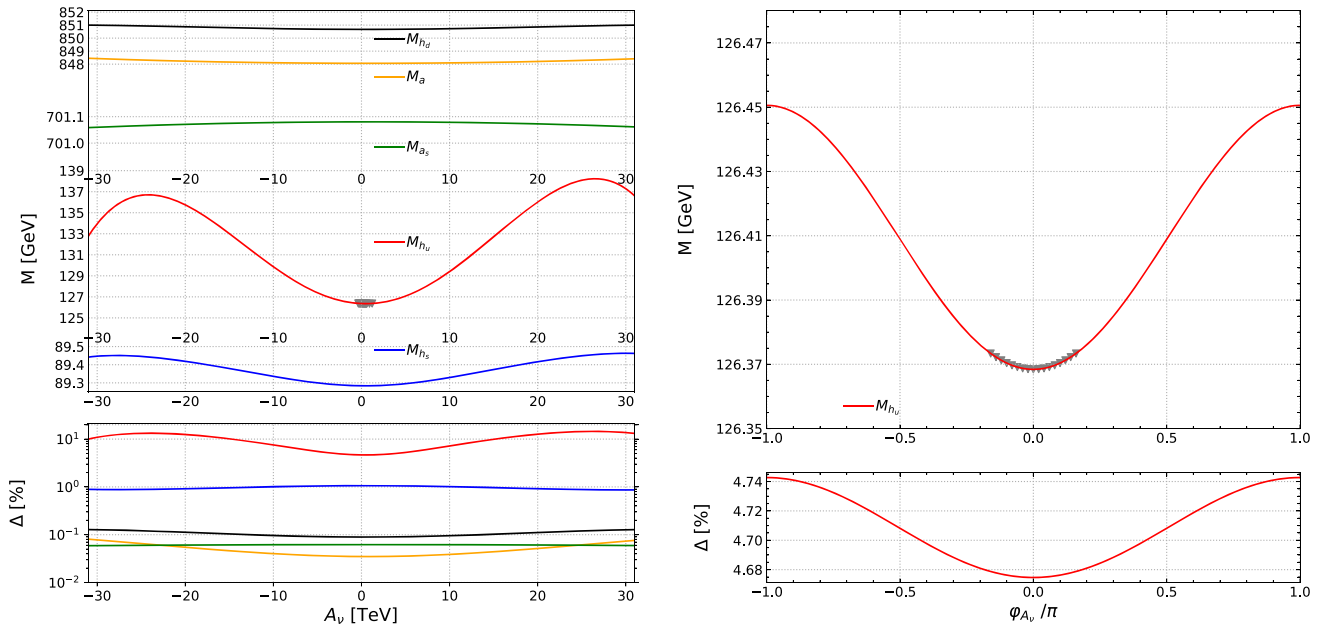

Fig. 5 The same as Fig. 4 but now we show the dependence on: **a** the neutrino trilinear coupling parameter A_ν and **b** the complex phase of A_ν. The gray triangles denote the points satisfying our constraints

the loop-corrected mass of the h_u-like Higgs boson, since the impact of the complex phase on the other Higgs boson masses is negligible. As can be inferred from the plots, the loop-corrected h_u-like Higgs boson mass is strongly affected by A_ν. This dependence looks like the dependence on the top trilinear coupling A_t and its complex phase, see for example [32,33], but the relative size of the corrections can cover a larger range if $Y_\nu^{\max}$ is large. The correction Δ_{h_u} is about 4.7% at $A_\nu = 0$ and maximal (14.5%) at $A_\nu \approx \pm 26$ TeV. The h_s-like Higgs boson mass depends slightly on A_ν while the other Higgs boson masses are barely affected by the variation of A_ν. We remind the reader that the maximum value of Y_ν that is obtained during the variation of A_ν is given by $Y_\nu^{\max} = 1.15$. In our analysis we also reduced $Y_\nu^{\max}$ to 0.8 by setting $\lambda_X = 1.33 \times 10^{-9}$ and varying A_ν. We then obtained the variation of Δ_{h_u} in the range [2, 3.6]%. In the right panel of Fig. 5, we observe a change of 0.08% for Δ_{h_u} when the complex phase φ_{A_ν} is varied in the range $[-\pi, \pi]$. Other complex phases of the neutrino sector like δ_{CP}, of the phases of λ_X, and μ_X have an insignificant impact on the loop-corrected Higgs masses.

Note that in Figs. 4 and 5 we present parameter points that satisfy all constraints by the gray area, respectively, the gray triangles. The other points violate charged flavor-violating lepton decays, the S, T, U parameters and/or the Higgs data.

In the remainder of this section, we present scatter plots in Fig. 6 which we obtained from our scan keeping only parameter points that satisfy all our mentioned constraints. The points are depicted in two-dimensional planes with M_X on the x-axis and μ_X on the y-axis. Note that M_X is related to λ_X and v_s as given in (2.31). Since λ_X and v_s are both varied in the scan, M_X may be a more appropriate parameter than λ_X for the scatter plots. The color code in the plot quantifies the size of the relative corrections Δ for the respective Higgs boson in the individual plots. The light gray points denote $\Delta \leq 0.2\%$, gray $0.2\% < \Delta \leq 0.5\%$, violet $0.5\% < \Delta \leq 1\%$, purple $1\% < \Delta \leq 2\%$, yellow $2\% < \Delta \leq 5\%$, orange $5\% < \Delta \leq 10\%$ and green $10\% < \Delta \leq 20\%$. The left plot of the Fig. 6 presents the relative corrections for the h_u-like Higgs boson, while the right plot for the h_d-like state. The Δ for the other Higgs bosons are less significant and therefore we do not present them here.

Most of the points obtained in our scan have small relative corrections $\Delta \leq 0.2\%$. Larger relative corrections are realized for μ_X-M_X towards the top-left corner of each plot, corresponding to increasing values of $Y_\nu^{\max}$. In the top-left corner, there are no points because they either violate the perturbativity constraint of $Y_\nu^{\max} < \sqrt{4\pi}$ or they lead to unstable numerical results due to large corrections. The color pattern is rather clear for the h_u-like Higgs boson, which confirms our conclusion on the strong dependence of Δ_{h_u} on $Y_\nu^{\max}$. There are some outliers which do not lie in their color bands, since Δ_{h_u} depends not only on $Y_\nu^{\max}$ but also on the sneutrino soft SUSY breaking parameters.

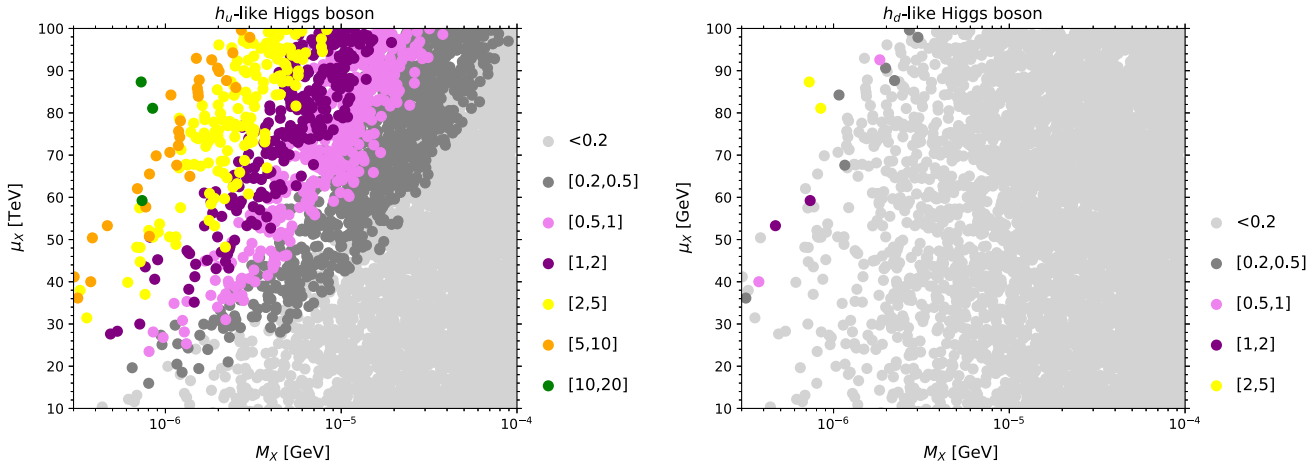

Fig. 6 Scatter plots in the plain of two variables of the neutrino sector, (M_X, μ_X) for the h_u-like (left) and the h_d-like (right) Higgs boson. The color code indicates the relative correction Δ (defined in (5.106)) for each Higgs state in percent

5.2 Impact of the (s)neutrinos on the LFV decays

In this section, we investigate the impact of the neutrinos and sneutrinos in the NMSSM with ISS on the radiative $l_1 \to l_2\gamma$ decays. As explained in Sect. 4.4, we consider three decay processes, namely $\mu \to e\gamma$, $\tau \to e\gamma$, and $\tau \to \mu\gamma$ among which the most stringent constraint exists for the decay $\mu \to e\gamma$. For all processes, the dominant contributions arise from the right-handed form factors F_R. The ratio between the contributions from the right- and left-handed form factors is approximately proportional to the ratio $m_{l_1}^2/m_{l_2}^2$ as can be inferred from the analytic expressions in Appendix A. One can therefore safely neglect the contribution from the left-handed form factors. We have divided the contributions to the form factors into three parts given by $F_{L,R}^{W^\pm}$, $F_{L,R}^{H^\pm}$, and $F_{L,R}^{\tilde{\chi}^\pm}$.

In our scan, the constraint on $\mu \to e\gamma$ is very important and rules out many points. The branching ratios are very sensitive to the spectrum of the neutrino and sneutrino sectors. In particular, they increase when the mixings between sterile neutrinos and active neutrinos increase. Both μ_X and λ_X have strong impacts on these mixings. We investigate this dependence by taking the parameter point `P1` of the previous section and varying again the parameters μ_X and λ_X.

In the left plot of Fig. 7, we show the dependence of the branching ratio (red line) for the decay $\mu \to e\gamma$ on λ_X. We also depict the individual contributions from the squared form factors $(F_{L,R}^x)^2$ with $x = W^\pm$ (black), $H^\pm$ (blue), and $\tilde{\chi}^\pm$ (orange) lines, as well as the interference terms $2(F_{L,R}^x)(F_{L,R}^y)$ with $(x, y) = (W^\pm, H^\pm)$ (green) $(W^\pm, \tilde{\chi}^\pm)$ (purple), and $(H^\pm, \tilde{\chi}^\pm)$ (yellow). For this parameter point scenarios, we find that the contributions from the W boson and from the charged Higgs boson are dominant, and the interference term between the W boson and charged Higgs form factors adds a significant contribution to the sum. We observed that the form factors $F_{L,R}^{W^\pm}$ and $F_{L,R}^{H^\pm}$ have the same sign while they are opposite in sign compared to $F_{L,R}^{\tilde{\chi}^\pm}$. The chargino contributions hence suppress the total decay widths. In the right plot of Fig. 7, we present the branching ratios for the three considered decay processes, $\mu \to e\gamma$, $\tau \to e\gamma$, and $\tau \to \mu\gamma$. We observe that the branching ratio for the process $\mu \to e\gamma$ is larger than for the other two processes. While the contributions from the W boson and charged Higgs form factors depend only on the spectrum and mixing of the neutrinos, the chargino contributions depend on those of the sneutrinos. One can vary the parameters of the sneutrino sector such as $m_{\tilde{N}}$ and $m_{\tilde{X}}$ to change the sign and the magnitude of the chargino contributions. We show the dependence of the branching ratio (red line) for the decay $\mu \to e\gamma$ on $m_{\tilde{N}}$ and $m_{\tilde{X}}$ in the left and right plot of Fig. 8, respectively.

We now investigate the impact of the parameters in the neutrino sector on the S, T, U parameters (STU), on the LFV decays and on the non-unitary 3×3 neutrino mixing matrix (NoU) discussed in Sect. 4.2. We started from the parameter point `P1` and we changed only the following parameters in the corresponding ranges,

$$\mu_X \in [10, 10^5]\,\text{GeV}, \quad \lambda_X \in [10^{-14}, 10^{-4}]. \tag{5.109}$$

All remaining parameters are kept fixed. We show in Fig. 9 a scatter plot in the plane of μ_X and λ_X. We have considered also the `HiggsBounds` and the `HiggsSignals` constraints, but simply not shown in this particular plot since we want to focus on the three mentioned constraints. The gray color denotes points which pass all three constraints while dark gray reflects points that violate all three constraints. The orange and green colors are for points violating STU and LFV constraints, respectively. The pink and yellow points, respectively, violate combinations of two constraints, namely LFV-STU and LFV-NoU. The white area on the plot

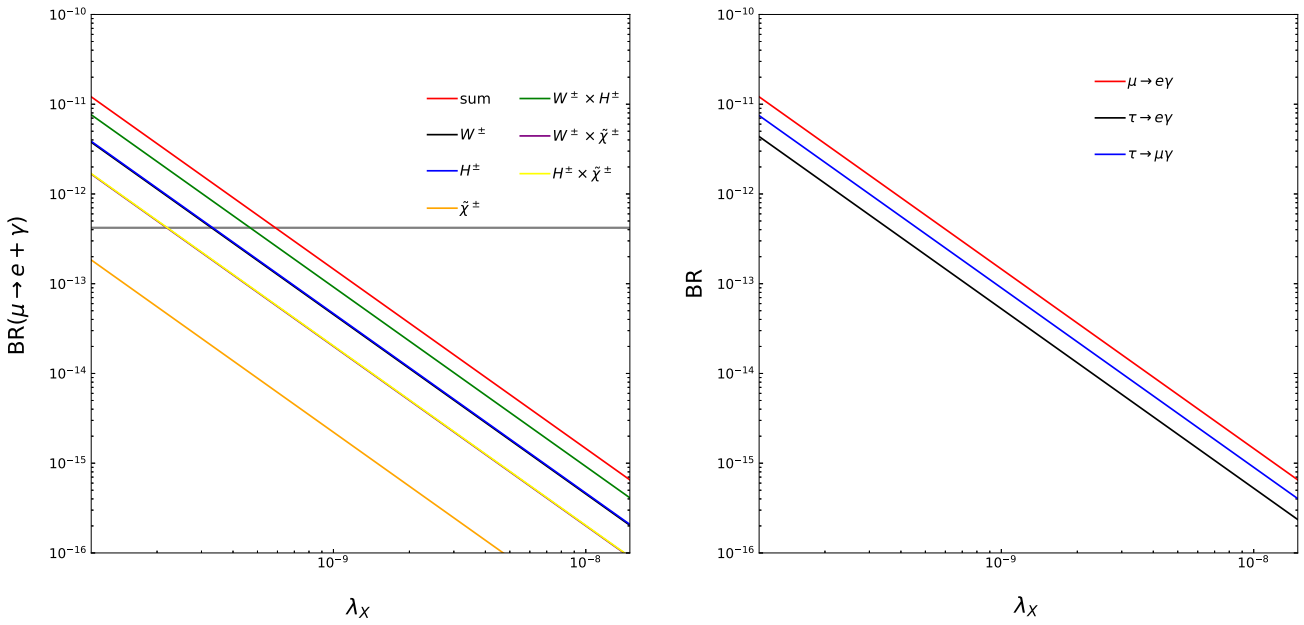

Fig. 7 Left: Branching ratio and its individual contributions for the decay $\mu \to e\gamma$ as a function of λ_X. The interference contributions $W^\pm \times \tilde{\chi}^\pm$ between the chargino and the $W^\pm$ form factors (violet), and $H^\pm \times \tilde{\chi}^\pm$ between the chargino and charged Higgs form factors (yellow) are negative. In order to present them in one plot we have changed the sign. The black line for $W^\pm$ is hidden under the blue line and the purple line is under the yellow one. The horizontal black line shows the experimental upper limit on the branching ratio. Right: Branching ratios for the three decays $\mu \to e\gamma$ (red), $\tau \to e\gamma$ (black), and $\tau \to \mu\gamma$ (blue) as function of λ_X

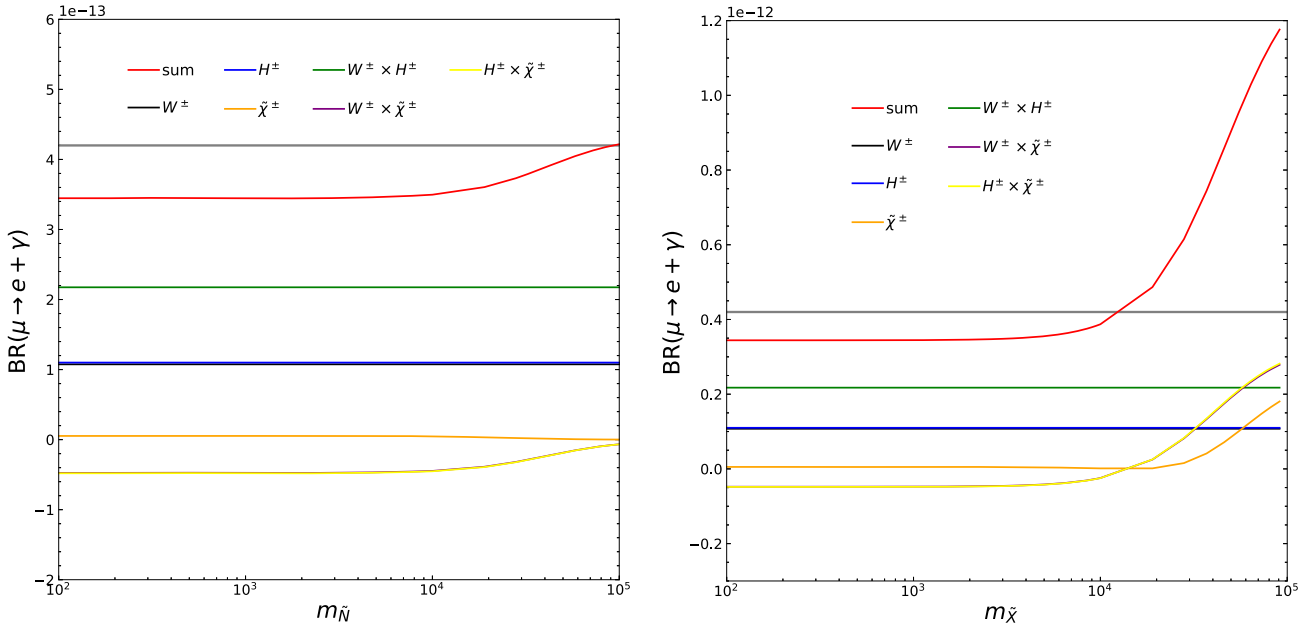

Fig. 8 Same as the left plot of Fig. 8, but $m_{\tilde{N}}$ (left) and $m_{\tilde{\chi}}$ (right) are varied instead

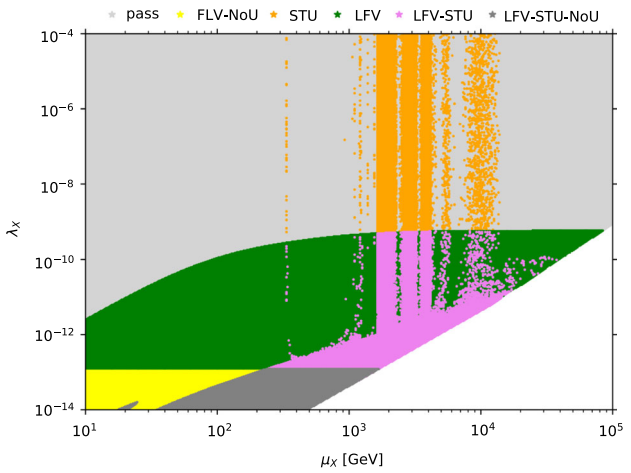

Fig. 9 Scatter plot in the μ_X and λ_X plane starting from the parameter point `P1`. The color code is used to distinguish between points that pass all three constraints LFV, STU, NoU (light gray), that do not pass any of the three constraints (dark gray) and that violate individual constraints or combinations of two constraints: LFV (green), STU (orange), LFV and STU (pink), LFV and NoU (yellow). See text for details

is not accessible since we encounter either negative values for one of the Higgs boson masses or $Y_\nu^{\max} > \sqrt{4\pi}$. As can be inferred from the plot, small values of λ_X ($\lesssim 10^{-12}$) are not preferred, independent of μ_X, since this parameter region is very sensitive to the constraints from LFV and NoU. For $\lambda_X > 10^{-12}$, the STU constraint is important in the region $\mu_X \in [10^3, 10^4]$ GeV and for $\mu_X = 320$ GeV, independent of λ_X. There are also regions such as $\mu_X < 300$ GeV or $\mu_X > 20$ TeV with $\lambda_X > 8 \times 10^{-10}$ where the three mentioned constraints do not play a role. This plot demonstrates the importance of taking into account the STU and LFV constraints when performing numerical analysis. Although the magnitude of λ_X signifies the magnitude of charged lepton flavor violation, *i.e.* the larger λ_X is the more violation we would expect, the reverse happens here. The reason is as follows. When we fix light neutrino masses m_ν, λ_X becomes inversely proportional to y_ν. Smaller λ_X, or larger y_ν, yields a larger mixing between sterile and active neutrinos, or a weaker GIM mechanism, and thus a larger LFV decay rate. This is also why small values of λ_X violate unitarity. Note that in our scan, we have assumed λ_X and μ_X to be diagonal. The results will change if these assumptions are not applied. Especially in the case where the off-diagonal components of y_ν are close to zero, and the LFV constraint is not as severe as in our case.

6 Conclusions

In this paper, we studied the impact of an extended neutrino sector on the NMSSM Higgs sector. We considered the framework of both the CP-conserving and CP-violating NMSSM extended by six singlet leptonic superfields. Their mixing with the three doublet leptonic superfields allows for the explanation of the tiny non-zero neutrino masses through the inverse seesaw mechanism. While R-parity is conserved in this model lepton number is explicitly violated through the interaction between two singlet neutrino superfields and a singlet Higgs superfield.

We quantified the indirect neutrino effects on the NMSSM Higgs sector by computing the complete one-loop corrections to the Higgs boson masses at non-vanishing external momentum. For the renormalization, we applied a mixed OS-$\overline{\text{DR}}$ scheme and consistently combined our one-loop result with the two-loop $\mathcal{O}(\alpha_t(\alpha_s + \alpha_t))$ results computed previously by our group. In the numerical analysis, we performed a parameter scan of the model and kept only those points for our study that respect the constraints from the Higgs data, the neutrino oscillation data, the charged lepton flavor-violating decays $l_i \to l_j + \gamma$, and the new physics constraints from the oblique parameters S, T, U. We presented the explicit calculation of the one-loop decay width for $l_i \to l_j + \gamma$. Our one-loop results have been implemented in the Fortran code `NMSSMCALC-nuSS`, that has been made publicly available and is based on the code `NMSSMCALC` that also computes the Higgs decays widths and branching ratios.

We found for our investigated benchmark point that the one-loop corrections from the neutrinos to the h_u-like, and hence SM-like, Higgs boson mass can shift its value by about 5%, decreasing slightly when the two-loop corrections are included, see Table 3. While the neutrino and sneutrino contributions come with opposite signs, their complete cancellation is prohibited by the soft-SUSY breaking terms in combination with electroweak symmetry breaking. We furthermore showed that a large neutrino Yukawa coupling has a significant impact on the loop corrections. The same is true for the soft-SUSY breaking trilinear coupling A_ν and its complex phase that affects the sneutrino sector while leaving the neutrino sector unchanged. Our findings on the dependence on the neutrino Yukawa coupling are confirmed by the presented scatter plots taking into account all of the parameter points passing the constraints. Large sterile neutrino masses, characterized by a large value of μ_X, can lead to large loop corrections due to the presence of the logarithmic term $\log \frac{\mu_X}{\mu_R}$. In case of a large ratio $\frac{\mu_X}{\mu_R}$ the reduction of the theoretical uncertainty is mandatory. This subject will be left for future study.

Our investigation of the one-loop corrected LFV decay $l_1 \to l_2\gamma$ shows that the constraints from this decay are relevant and need to be taken into account. This result is underlined by an analysis of the impact of all considered constraints that shows the importance of the S, T, U and LFV constraints on the validity of the parameter scenarios.

In summary, the one-loop analysis of the impact of an extended (s)neutrino sector on the NMSSM demonstrates

the importance of taking into account these indirect effects through loop contributions. Together with the usual constraints from Higgs data and new physics as well as from LFV decays, they constrain the valid parameter space of the model.

Acknowledgements The research of MM was supported by the Deutsche Forschungsgemeinschaft (DFG, German Research Foundation) under Grant 396021762-TRR 257. T.N.D is funded by the Vietnam National Foundation for Science and Technology Development (NAFOSTED) under Grant number 103.01-2020.17.

Data Availability Statement This manuscript has no associated data or the data will not be deposited. [Authors' comment: The experimental results are constantly updated so that the constraints and the allowed parameter points will evolve. We therefore prefer not to deposit the data. The data can be provided, however, upon request.]

Funded by SCOAP[3]. SCOAP[3] supports the goals of the International Year of Basic Sciences for Sustainable Development.

Appendix A: Form factors

In this appendix we give the left- and right-handed form factors for the LFV radiative decays $l_1 \to l_2 + \gamma$ discussed in Sect. 4.4. For simplicity, we introduce the following abbreviations for the one-loop three-point integrals

$$C^W_{i\ldots} = C_{i\ldots}\left(m_1^2, 0, m_2^2, m_{\nu_i}^2, M_W^2, M_W^2\right) \tag{A.110}$$

$$C^H_{i\ldots} = C_{i\ldots}\left(m_1^2, 0, m_2^2, m_{\nu_i}^2, M_{H^\pm}^2, M_{H^\pm}^2\right) \tag{A.111}$$

$$C^\chi_{i\ldots} = C_{i\ldots}\left(m_1^2, 0, m_2^2, m_{\tilde{n}_i}^2, m_{\tilde{\chi}_j^\pm}^2, m_{\tilde{\chi}_j^\pm}^2\right). \tag{A.112}$$

We use the following conventions,

$$C_0^W = \frac{(\mu_R^2\pi)^{(4-D)/2}}{i\pi^2}\int dq^D \frac{1}{D_x}, \tag{A.113}$$

$$C_1^W k_1^\mu + C_2^W k_2^\mu = \frac{(\mu_R^2\pi)^{(4-D)/2}}{i\pi^2}\int dq^D \frac{q^\mu}{D_x}, \tag{A.114}$$

$$\begin{aligned} &C_{00}^W g^{\mu\nu} + C_{11}^W k_1^\mu k_1^\nu + C_{12}^W (k_1^\mu k_2^\nu + k_1^\nu k_2^\mu) + C_{22}^W k_2^\mu k_2^\nu \\ &= \frac{(\mu_R^2\pi)^{(4-D)/2}}{i\pi^2}\int dq^D \frac{q^\mu q^\nu}{D_x}, \end{aligned} \tag{A.115}$$

where the denominator D_x is given by

$$D_x = (q^2 - m_{n_i}^2)((q-k_1)^2 - M_W^2)((q-k_2)^2 - M_W^2), \tag{A.116}$$

with $k_1^2 = m_1^2, k_2^2 = m_2^2$ and $(k_1 - k_2)^2 = 0$ and m_1 (m_2) denoting the l_1 (l_2) mass, m_{n_i} the mass of all the neutrinos, the active and the sterile ones.

In the 't Hooft–Feynman gauge, the left- and right-handed form factors, $F_{L,R}^{W^\pm,H^\pm,\chi^\pm}$, defined in (4.99) are given by

$$\begin{aligned} F_L^{W^\pm} = &\frac{e^3 m_2}{16\pi^2 M_W^2 s_W^2}\sum_{i=1}^{9} U_{\nu\, il_1} U_{\nu\, il_2}^* \\ &\times\Big[m_{n_i}^2\left(C_0^W + C_1^W + 2C_2^W + C_{12}^W + C_{22}^W\right) \\ &+ M_W^2\left(-2C_1^W + 2C_{12}^W \right. \\ &\left. +2C_{22}^W\right) + m_1^2\left(C_1^W + C_{11}^W + C_{12}^W\right)\Big] \end{aligned} \tag{A.117}$$

$$\begin{aligned} F_R^{W^\pm} = &\frac{e^3 m_1}{16\pi^2 M_W^2 s_W^2}\sum_{i=1}^{9} U_{\nu\, il_1} U_{\nu\, il_2}^* \\ &\times\Big[m_{n_i}^2\left(C_0^W + 2C_1^W + C_2^W + C_{11}^W + C_{12}^W\right) \\ &+ M_W^2\left(-2C_2^W + 2C_{11}^W + 2C_{12}^W\right) \\ &+ m_2^2\left(C_2^W + C_{12}^W + C_{22}^W\right)\Big], \end{aligned} \tag{A.118}$$

for the $W^\pm$ and charged Goldstone boson triangle diagrams,

$$\begin{aligned} F_L^{H^\pm} = &\frac{e^3 m_2}{16\pi^2 M_W^2 s_W^2}\sum_{i=1}^{9} U_{\nu\, il_1} U_{\nu\, il_2}^* \\ &\times\Big[m_{n_i}^2\left(-(C_0^{H^\pm} + C_1^{H^\pm} + C_2^{H^\pm}) \right. \\ &\left. +\frac{1}{t_\beta^2}(C_2^{H^\pm} + C_{12}^{H^\pm} + C_{22}^{H^\pm})\right) \\ &+ m_1^2 t_\beta^2\left(C_1^{H^\pm} + C_{11}^{H^\pm} + C_{12}^{H^\pm}\right)\Big] \end{aligned} \tag{A.119}$$

$$\begin{aligned} F_R^{H^\pm} = &\frac{e^3 m_1}{16\pi^2 M_W^2 s_W^2}\sum_{i=1}^{9} U_{\nu\, il_1} U_{\nu\, il_2}^* \\ &\times\Big[m_{n_i}^2\left(-(C_0^{H^\pm} + C_1^{H^\pm} + C_2^{H^\pm}) \right. \\ &\left. +\frac{1}{t_\beta^2}\left(C_1^{H^\pm} + C_{11}^{H^\pm} + C_{12}^{H^\pm}\right)\right) \\ &+ m_2^2 t_\beta^2\left(C_2^{H^\pm} + C_{12}^{H^\pm} + C_{22}^{H^\pm}\right)\Big], \end{aligned} \tag{A.120}$$

for the charged Higgs triangle diagram, and

$$F_L^{\tilde{\chi}^\pm} = -\frac{e}{8\pi^2}\sum_{i=1}^{18}\sum_{j=1}^{2} \times\Bigg[m_1 g^{L*}_{e_{l_1}^+\tilde{\chi}_j\tilde{\nu}_i} g^{L}_{e_{l_2}^+\tilde{\chi}_j\tilde{\nu}_i}\left(C_1^{\tilde{\chi}_j^\pm}+C_{12}^{\tilde{\chi}_j^\pm}+C_{11}^{\tilde{\chi}_j^\pm}\right) + m_{\tilde{\chi}_j^\pm} g^{R*}_{e_{l_1}^+\tilde{\chi}_j\tilde{\nu}_i} g^{L}_{e_{l_2}^+\tilde{\chi}_j\tilde{\nu}_i}\left(C_1^{\tilde{\chi}_j^\pm}+C_2^{\tilde{\chi}_j^\pm}\right) + m_2 g^{R*}_{e_{l_1}^+\tilde{\chi}_j\tilde{\nu}_i} g^{R}_{e_{l_2}^+\tilde{\chi}_j\tilde{\nu}_i}\left(C_2^{\tilde{\chi}_j^\pm}+C_{22}^{\tilde{\chi}_j^\pm}+C_{12}^{\tilde{\chi}_j^\pm}\right)\Bigg] \tag{A.121}$$

$$F_R^{\tilde{\chi}^\pm} = -\frac{e}{8\pi^2}\sum_{i=1}^{18}\sum_{j=1}^{2} \times\Bigg[m_2 g^{L*}_{e_{l_1}^+\tilde{\chi}_j\tilde{\nu}_i} g^{L}_{e_{l_2}^+\tilde{\chi}_j\tilde{\nu}_i}\left(C_2^{\tilde{\chi}_j^\pm}+C_{12}^{\tilde{\chi}_j^\pm}+C_{22}^{\tilde{\chi}_j^\pm}\right) + m_{\tilde{\chi}_j^\pm} g^{L*}_{e_{l_1}^+\tilde{\chi}_j\tilde{\nu}_i} g^{R}_{e_{l_2}^+\tilde{\chi}_j\tilde{\nu}_i}\left(C_1^{\tilde{\chi}_j^\pm}+C_2^{\tilde{\chi}_j^\pm}\right) + m_1 g^{R*}_{e_{l_1}^+\tilde{\chi}_j\tilde{\nu}_i} g^{R}_{e_{l_2}^+\tilde{\chi}_j\tilde{\nu}_i}\left(C_1^{\tilde{\chi}_j^\pm}+C_{11}^{\tilde{\chi}_j^\pm}+C_{12}^{\tilde{\chi}_j^\pm}\right)\Bigg], \tag{A.122}$$

for the triangle diagrams with sneutrinos and charginos in the internal lines. The left- and right-handed couplings between the leptons, charginos and sneutrinos are defined in the interaction Lagrangian,

$$\bar{e}_k\left(i g^{L}_{e_k^+\tilde{\chi}_j\tilde{\nu}_i} P_L + i g^{R}_{e_k^+\tilde{\chi}_j\tilde{\nu}_i} P_R\right)\chi_j^-\tilde{\nu}_i, \tag{A.123}$$

where

$$g^{L}_{e_k^+\tilde{\chi}_j\tilde{\nu}_i} = \frac{m_k}{v c_\beta}\left(U^{\tilde{\nu}}_{ik} + i U^{\tilde{\nu}}_{i(k+9)}\right)U^*_{j2} \tag{A.124}$$

$$g^{R}_{e_k^+\tilde{\chi}_j\tilde{\nu}_i} = -\frac{g_2 V_{j1}}{\sqrt{2}}\left(U^{\tilde{\nu}}_{ik} + i U^{\tilde{\nu}}_{i(k+9)}\right) + \frac{1}{\sqrt{2}} V_{j2}\sum_{n=1}^{3}\left(U^{\tilde{\nu}}_{i(n+3)} + i U^{\tilde{\nu}}_{i(n+12)}\right) Y^*_{\nu,kn}. \tag{A.125}$$

In the numerical analysis we used the massless limit for the external lines. In this limit, one has the following simple expressions for the one-loop three-point integrals [70]

$$C_0(0,0,0,x,y,y) = \frac{1}{x}\left(-\frac{1}{t-1}+\frac{\ln(t)}{(t-1)^2}\right) \tag{A.126}$$

$$C_1(0,0,0,x,y,y) = \frac{1}{x}\left(\frac{(t-3)}{4(t-1)^2}+\frac{\ln(t)}{2(t-1)^3}\right) \tag{A.127}$$

$$C_{11}(0,0,0,x,y,y) = \frac{1}{x}\left(\frac{(-2t^2+7t-11)}{18(t-1)^3}+\frac{\ln(t)}{3(t-1)^4}\right) \tag{A.128}$$

$$C_2(0,0,0,x,y,y) = C_1(0,0,0,x,y,y) \tag{A.129}$$

$$C_{22}(0,0,0,x,y,y) = 2C_{12}(0,0,0,x,y,y) = C_{11}(0,0,0,x,y,y), \tag{A.130}$$

where $t = y/x$.

Appendix B: Sneutrino mass matrix

The mass matrix of the sneutrinos written in each 3×3 block is given by

$$(M_{\tilde{\nu}})_{\tilde{\nu}_+\tilde{\nu}_+} = \frac{1}{2} I_3 M_z^2\cos 2\beta + \frac{1}{2}\left(\tilde{m}_L^2+\tilde{m}_L^{2T}\right) + \frac{1}{2} v_u^2 \mathrm{Re}\left(y_\nu y_\nu^\dagger\right) \tag{B.131}$$

$$(M_{\tilde{\nu}})_{\tilde{\nu}_+\tilde{N}_+} = \frac{1}{\sqrt{2}} v_u \mathrm{Re}\left(e^{i\varphi_u} y_\nu A_\nu\right) - \frac{1}{2} v_d v_s \mathrm{Re}\left((e^{i\varphi_s}\lambda y_\nu^*\right) \tag{B.132}$$

$$(M_{\tilde{\nu}})_{\tilde{\nu}_+\tilde{X}_+} = \frac{1}{\sqrt{2}} v_u \mathrm{Re}\left(e^{i\varphi_u} y_\nu \mu_X^*\right) \tag{B.133}$$

$$(M_{\tilde{\nu}})_{\tilde{\nu}_+\tilde{\nu}_-} = \frac{i}{2}\left(\tilde{m}_L^2-\tilde{m}_L^{2T}\right) + \frac{1}{2} v_u^2 \Im\left(y_\nu y_\nu^\dagger\right) \tag{B.134}$$

$$(M_{\tilde{\nu}})_{\tilde{\nu}_+\tilde{N}_-} = \frac{1}{\sqrt{2}} v_u \Im\left(e^{i\varphi_u} y_\nu A_\nu\right) - \frac{1}{2} v_d v_s \Im\left(e^{i\varphi_s}\lambda y_\nu^*\right) \tag{B.135}$$

$$(M_{\tilde{\nu}})_{\tilde{\nu}_+\tilde{X}_-} = \frac{1}{\sqrt{2}} v_u \Im\left(e^{i\varphi_u} y_\nu \mu_X^*\right) \tag{B.136}$$

$$(M_{\tilde{\nu}})_{\tilde{N}_+\tilde{N}_+} = \frac{1}{2}\left(\tilde{m}_N^2+\tilde{m}_N^{2T}\right) + \mathrm{Re}\left(\mu_X\mu_X^\dagger\right) + \frac{1}{2} v_u^2 \mathrm{Re}\left(y_\nu^T y_\nu^*\right) \tag{B.137}$$

$$(M_{\tilde{\nu}})_{\tilde{N}_+\tilde{X}_+} = \mathrm{Re}\left(\mu_X B_{\mu_X}\right) + \frac{1}{\sqrt{2}} v_s \mathrm{Re}\left[e^{-i\varphi_s}\mu_X\left(\lambda_X^\dagger+\lambda_X^*\right)\right] \tag{B.138}$$

$$(M_{\tilde{\nu}})_{\tilde{N}_+\tilde{\nu}_-} = -\frac{1}{\sqrt{2}} v_u \Im\left(e^{i\varphi_u} A_\nu^T y_\nu^T\right) - \frac{1}{2} v_d v_s \Im\left(e^{i\varphi_s}\lambda y_\nu^\dagger\right) \tag{B.139}$$

$$(M_{\tilde{\nu}})_{\tilde{N}_+\tilde{N}_-} = \frac{i}{2}\left(\tilde{m}_N^2-\tilde{m}_N^{2T}\right) - \Im\left(\mu_X\mu_X^\dagger\right) - \frac{1}{2} v_u^2 \Im\left(y_\nu^T y_\nu^*\right) \tag{B.140}$$

$$(M_{\tilde{\nu}})_{\tilde{N}_+\tilde{X}_-} = -\Im\left(\mu_X B_{\mu_X}\right) + \frac{1}{\sqrt{2}} v_s \Im\left[e^{-i\varphi_s}\mu_X\left(\lambda_X^\dagger+\lambda_X^*\right)\right] \tag{B.141}$$

$$(M_{\tilde{\nu}})_{\tilde{X}_+\tilde{X}_+} = \frac{1}{2}\left(\tilde{m}_X^2+\tilde{m}_X^{2T}\right) + \mathrm{Re}\left(\mu_X^T\mu_X^*\right) + \frac{1}{2}\mathrm{Re}\left[\left(e^{2i\varphi_s} v_s^2\kappa - e^{i\varphi_u} v_d v_u\lambda\right)\left(\lambda_X^*+\lambda_X^\dagger\right)\right] + \frac{1}{2} v_s^2 \mathrm{Re}\left[\left(\lambda_X+\lambda_X^T\right)\left(\lambda_X^\dagger+\lambda_X^*\right)\right] + \frac{1}{\sqrt{2}} v_s \mathrm{Re}\left[e^{i\varphi_s}\left(\lambda_X A_X + A_X^T\lambda_X^T\right)\right] \tag{B.142}$$

$$(M_{\tilde{\nu}})_{\tilde{X}_+\tilde{\nu}_-} = -\frac{1}{\sqrt{2}} v_u \Im\left(e^{i\varphi_u}\mu_X^\dagger y_\nu^T\right) \tag{B.143}$$

$$(M_{\tilde{\nu}})_{\tilde{X}_+\tilde{N}_-} = \Im\left(B_{\mu_X}^T\mu_X^T\right)$$

$$+\frac{1}{\sqrt{2}}v_s\Im\left[e^{-i\varphi_s}\left(\lambda_X^\dagger+\lambda_X^*\right)\mu_X^T\right] \tag{B.144}$$

$$\begin{aligned}(M_{\tilde{\nu}})_{\tilde{X}_+\tilde{X}_-} &= \frac{i}{2}\left(\tilde{m}_X^2-\tilde{m}_X^{2T}\right)\\ &+\Im\left(\mu_X^T\mu_X^*\right)\\ &+\frac{1}{2}\Im\left[\left(e^{2i\varphi_s}v_s^2\kappa-e^{i\varphi_u}v_dv_u\lambda\right)\left(\lambda_X^*+\lambda_X^\dagger\right)\right]\\ &+\frac{1}{2}v_s^2\Im\left[\left(\lambda_X+\lambda_X^T\right)\left(\lambda_X^\dagger+\lambda_X^*\right)\right]\\ &-\frac{1}{\sqrt{2}}v_s\Im\left[e^{i\varphi_s}\left(\lambda_XA_X+A_X^T\lambda_X^T\right)\right]\end{aligned} \tag{B.145}$$

$$(M_{\tilde{\nu}})_{\tilde{\nu}_-\tilde{\nu}_-} = \frac{1}{2}I_3M_z^2\cos 2\beta+\frac{1}{2}\left(\tilde{m}_L^2+\tilde{m}_L^{2T}\right)+\frac{1}{2}v_u^2\mathrm{Re}\left(y_\nu y_\nu^\dagger\right) \tag{B.146}$$

$$(M_{\tilde{\nu}})_{\tilde{\nu}_-\tilde{N}_-} = \frac{1}{\sqrt{2}}v_u\mathrm{Re}\left(e^{i\varphi_u}y_\nu A_\nu\right)-\frac{1}{2}v_dv_s\mathrm{Re}\left(e^{i\varphi_s}\lambda y_\nu^*\right) \tag{B.147}$$

$$(M_{\tilde{\nu}})_{\tilde{\nu}_-\tilde{X}_-} = \frac{1}{\sqrt{2}}v_u\mathrm{Re}\left(e^{i\varphi_u}y_\nu\mu_X^*\right) \tag{B.148}$$

$$(M_{\tilde{\nu}})_{\tilde{N}_-\tilde{N}_-} = \frac{1}{2}\left(\tilde{m}_N^2+\tilde{m}_N^{2T}\right)+\mathrm{Re}\left(\mu_X\mu_X^\dagger\right)+\frac{1}{2}v_u^2\mathrm{Re}\left(y_\nu^Ty_\nu^*\right) \tag{B.149}$$

$$(M_{\tilde{\nu}})_{\tilde{N}_-\tilde{X}_-} = \mathrm{Re}\left(\mu_XB_{\mu_X}\right)-\frac{1}{\sqrt{2}}v_s\mathrm{Re}\left[e^{-i\varphi_s}\mu_X\left(\lambda_X^\dagger+\lambda_X^*\right)\right] \tag{B.150}$$

$$\begin{aligned}(M_{\tilde{\nu}})_{\tilde{X}_-\tilde{X}_-} &= \frac{1}{2}\left(\tilde{m}_X^2+\tilde{m}_X^{2T}\right)+\mathrm{Re}\left(\mu_X^T\mu_X^*\right)\\ &-\frac{1}{2}\mathrm{Re}\left[\left(e^{2i\varphi_s}v_s^2\kappa-e^{i\varphi_u}v_dv_u\lambda\right)\left(\lambda_X^*+\lambda_X^\dagger\right)\right]\\ &+\frac{1}{2}v_s^2\mathrm{Re}\left[\left(\lambda_X+\lambda_X^T\right)\left(\lambda_X^\dagger+\lambda_X^*\right)\right]\\ &-\frac{1}{\sqrt{2}}v_s\mathrm{Re}\left[e^{i\varphi_s}\left(\lambda_XA_X+A_X^T\lambda_X^T\right)\right].\end{aligned} \tag{B.151}$$

Appendix C: Neutral Higgs mass matrix counterterm

In this section we present the counterterm mass matrix for the neutral Higgs bosons in the basis $(h_d, h_u, h_s, a, a_s)^T$. We use the convention $\varphi_y = \varphi_\kappa - \varphi_\lambda + 2\varphi_s - \varphi_u, \varphi_\omega = \varphi_\kappa + 3\varphi_s$ and the short-hand notation $s_x \equiv \sin x, c_x \equiv \cos x$.

$$\begin{aligned}&\left(\delta^{(1)}M_{hh}\right)_{h_dh_d}\\ &= c_\beta^3s_\beta\delta^{(1)}t_\beta\left(v^2|\lambda|^2-2M_W^2-2M_Z^2+2M_{H^\pm}^2\right)\\ &+v^2|\lambda|s_\beta^2\delta^{(1)}|\lambda|+v|\lambda|^2s_\beta^2\delta^{(1)}v-\frac{\left(c_{2\beta}-3\right)c_\beta\delta^{(1)}t_{h_d}}{2v}\\ &-\frac{c_\beta^2s_\beta\delta^{(1)}t_{h_u}}{v}+c_\beta^2\delta^{(1)}M_Z^2-s_\beta^2\delta^{(1)}M_W^2+\delta^{(1)}M_{H^\pm}^2s_\beta^2\end{aligned} \tag{C.152}$$

$$\begin{aligned}&\left(\delta^{(1)}M_{hh}\right)_{h_dh_u}\\ &= \frac{1}{2}c_{2\beta}c_\beta^2\delta^{(1)}t_\beta\left(v^2|\lambda|^2+2M_W^2-2M_Z^2-2M_{H^\pm}^2\right)\\ &+v^2|\lambda|c_\beta s_\beta\delta^{(1)}|\lambda|+v|\lambda|^2c_\beta s_\beta\delta^{(1)}v+\frac{c_\beta^3\delta^{(1)}t_{h_u}}{v}\\ &+c_\beta s_\beta\delta^{(1)}M_W^2-c_\beta s_\beta\delta^{(1)}M_Z^2\\ &-c_\beta\delta^{(1)}M_{H^\pm}^2s_\beta+\frac{s_\beta^3\delta^{(1)}t_{h_d}}{v}\end{aligned} \tag{C.153}$$

$$\begin{aligned}&\left(\delta^{(1)}M_{hh}\right)_{h_dh_s} = -\frac{vc_\beta^2\delta^{(1)}t_\beta}{2v_s}\left(2c_\beta^2s_\beta\left(v^2|\lambda|^2-2M_W^2+2M_{H^\pm}^2\right)+|\kappa|\right.\\ &\left.\times|\lambda|c_\beta v_s^2c_{\varphi_y}+s_\beta^3\left(-\left(v^2|\lambda|^2-2M_W^2+2M_{H^\pm}^2\right)\right)+2|\lambda|^2s_\beta v_s^2\right)\\ &+\frac{v\delta^{(1)}v_s\left(c_\beta\left(s_\beta^2\left(v^2|\lambda|^2-2M_W^2\right)+2|\lambda|^2v_s^2\right)+s_\beta\left(M_{H^\pm}^2s_{2\beta}-|\kappa||\lambda|v_s^2c_{\varphi_y}\right)\right)}{2v_s^2}\\ &+\frac{\delta^{(1)}v\left(s_\beta\left(M_W^2s_{2\beta}-|\kappa||\lambda|v_s^2c_{\varphi_y}\right)+c_\beta\left(2|\lambda|^2v_s^2-s_\beta^2\left(3v^2|\lambda|^2+2M_{H^\pm}^2\right)\right)\right)}{2v_s}\\ &+\delta^{(1)}|\lambda|\left(c_\beta\left(2v|\lambda|v_s-\frac{v^3|\lambda|s_\beta^2}{v_s}\right)-\frac{1}{2}v|\kappa|s_\beta v_sc_{\varphi_y}\right)-\frac{1}{2}v|\lambda|s_\beta v_s\delta^{(1)}|\kappa|c_{\varphi_y}+\frac{1}{2}v|\kappa||\lambda|s_\beta v_ss_{\varphi_y}\delta^{(1)}\varphi_y\\ &+\frac{c_\beta^3s_\beta\delta^{(1)}t_{h_u}}{v_s}+\frac{vc_\beta s_\beta^2\delta^{(1)}M_W^2}{v_s}-\frac{vc_\beta\delta^{(1)}M_{H^\pm}^2s_\beta^2}{v_s}+\frac{s_\beta^4\delta^{(1)}t_{h_d}}{v_s}\end{aligned} \tag{C.154}$$

$$\left(\delta^{(1)}M_{hh}\right)_{h_d a} = \frac{\delta^{(1)}t_{a_d}\cot\beta}{v} \tag{C.155}$$

$$\left(\delta^{(1)}M_{hh}\right)_{h_d a_s} = \frac{\delta^{(1)}t_{a_d}}{v_s} + \frac{3}{2}v\,|\kappa|\,|\lambda|\,c_\beta^3 v_s s_{\varphi_y}\delta^{(1)}t_\beta + \frac{3}{2}v\,|\kappa|\,|\lambda|\,s_\beta v_s c_{\varphi_y}\delta^{(1)}\varphi_y + \frac{3}{2}v\,|\lambda|\,s_\beta v_s\delta^{(1)}|\kappa|s_{\varphi_y}$$
$$+ \frac{3}{2}v\,|\kappa|\,s_\beta v_s\delta^{(1)}|\lambda|s_{\varphi_y} + \frac{3}{2}v\,|\kappa|\,|\lambda|\,s_\beta\delta^{(1)}v_s s_{\varphi_y} + \frac{3}{2}\,|\kappa|\,|\lambda|\,s_\beta v_s\delta^{(1)}v s_{\varphi_y} \tag{C.156}$$

$$\left(\delta^{(1)}M_{hh}\right)_{h_u h_u} = c_\beta^3 s_\beta\delta^{(1)}t_\beta\left(-v^2\,|\lambda|^2 + 2M_W^2 + 2M_Z^2 - 2M_{H^\pm}^2\right) + v^2\,|\lambda|\,c_\beta^2\delta^{(1)}|\lambda| + v\,|\lambda|^2\,c_\beta^2\delta^{(1)}v - \frac{c_\beta s_\beta^2\delta^{(1)}t_{h_d}}{v}$$
$$+ \frac{\left(c_{2\beta}+3\right)s_\beta\delta^{(1)}t_{h_u}}{2v} - c_\beta^2\delta^{(1)}M_W^2 + c_\beta^2\delta^{(1)}M_{H^\pm}^2 + s_\beta^2\delta^{(1)}M_Z^2 \tag{C.157}$$

$$\left(\delta^{(1)}M_{hh}\right)_{h_u h_s} = \frac{v c_\beta^2\delta^{(1)}t_\beta}{2v_s}\left(2c_\beta\left(|\lambda|^2 v_s^2 + 2s_\beta^2\left(M_{H^\pm}^2 - M_W^2\right)\right) + c_\beta^3\left(-\left(v^2\,|\lambda|^2 - 2M_W^2 + 2M_{H^\pm}^2\right)\right)\right.$$
$$\left. + |\lambda|\,s_\beta\left(|\kappa|\,v_s^2 c_{\varphi_y} + v^2\,|\lambda|\,s_{2\beta}\right)\right) + \frac{1}{2}v\delta^{(1)}v_s\left(\frac{c_\beta^2 s_\beta\left(v^2\,|\lambda|^2 - 2M_W^2 + 2M_{H^\pm}^2\right)}{v_s^2} - |\kappa|\,|\lambda|\,c_\beta c_{\varphi_y} + 2\,|\lambda|^2\,s_\beta\right)$$
$$+ \delta^{(1)}v\left(-\frac{c_\beta^2 s_\beta\left(3v^2\,|\lambda|^2 - 2M_W^2 + 2M_{H^\pm}^2\right)}{2v_s} - \frac{1}{2}\,|\kappa|\,|\lambda|\,c_\beta v_s c_{\varphi_y} + |\lambda|^2\,s_\beta v_s\right) + \delta^{(1)}|\lambda|\left(-\frac{v^3\,|\lambda|\,c_\beta^2 s_\beta}{v_s}\right.$$
$$\left. - \frac{1}{2}v\,|\kappa|\,c_\beta v_s c_{\varphi_y} + 2v\,|\lambda|\,s_\beta v_s\right) - \frac{1}{2}v\,|\lambda|\,c_\beta v_s\delta^{(1)}|\kappa|c_{\varphi_y} + \frac{1}{2}v\,|\kappa|\,|\lambda|\,c_\beta v_s s_{\varphi_y}\delta^{(1)}\varphi_y + \frac{c_\beta s_\beta^3\delta^{(1)}t_{h_d}}{v_s}$$
$$+ \frac{c_\beta^4\delta^{(1)}t_{h_u}}{v_s} + \frac{v c_\beta^2 s_\beta\delta^{(1)}M_W^2}{v_s} - \frac{v c_\beta^2\delta^{(1)}M_{H^\pm}^2 s_\beta}{v_s} \tag{C.158}$$

$$\left(\delta^{(1)}M_{hh}\right)_{h_u a} = \frac{\delta^{(1)}t_{a_d}}{v} \tag{C.159}$$

$$\left(\delta^{(1)}M_{hh}\right)_{h_u a_s} = \frac{\cot\beta\,\delta^{(1)}t_{a_d}}{v_s} - \frac{3}{2}v\,|\kappa|\,|\lambda|\,c_\beta^2 s_\beta v_s s_{\varphi_y}\delta^{(1)}t_\beta + \frac{3}{2}v\,|\lambda|\,c_\beta v_s\delta^{(1)}|\kappa|s_{\varphi_y} + \frac{3}{2}v\,|\kappa|\,c_\beta v_s\delta^{(1)}|\lambda|s_{\varphi_y}$$
$$+ \frac{3}{2}v\,|\kappa|\,|\lambda|\,c_\beta\delta^{(1)}v_s s_{\varphi_y} + \frac{3}{2}v\,|\kappa|\,|\lambda|\,c_\beta v_s c_{\varphi_y}\delta^{(1)}\varphi_y + \frac{3}{2}\,|\kappa|\,|\lambda|\,c_\beta v_s\delta^{(1)}v s_{\varphi_y} \tag{C.160}$$

$$\left(\delta^{(1)}M_{hh}\right)_{h_s h_s} = -\frac{v s_\beta\delta^{(1)}t_{h_u}c_\beta^4}{v_s^2} + \frac{v^2 s_\beta^2\delta^{(1)}M_{H^\pm}^2 c_\beta^2}{v_s^2} - \frac{v^2 s_\beta^2\delta^{(1)}M_W^2 c_\beta^2}{v_s^2} + \frac{1}{2}v^2 c_{2\beta}$$
$$\times\left(-|\kappa|\,|\lambda|\,c_{\varphi_y} + \frac{3i\left(-1+e^{2i\varphi_\omega}\right)|\kappa|\,|\lambda|\,s_{\varphi_y}}{1+e^{2i\varphi_\omega}} + \frac{\left(v^2\,|\lambda|^2 - 2M_W^2 + 2M_{H^\pm}^2\right)s_{2\beta}}{v_s^2}\right)\delta^{(1)}t_\beta c_\beta^2 + \frac{i\left(-1+e^{2i\varphi_\omega}\right)v\delta^{(1)}t_{a_d}c_\beta}{\left(1+e^{2i\varphi_\omega}\right)v_s^2}$$
$$- \frac{v s_\beta^4\delta^{(1)}t_{h_d}c_\beta}{v_s^2} + \frac{v^2\,|\kappa|\,|\lambda|\,s_\beta\left(3i\left(-1+e^{2i\varphi_\omega}\right)c_{\varphi_y} + \left(1+e^{2i\varphi_\omega}\right)s_{\varphi_y}\right)\delta^{(1)}\varphi_y c_\beta}{2\left(1+e^{2i\varphi_\omega}\right)}$$
$$+ \frac{1}{2}v\delta^{(1)}v s_{2\beta}\left(-|\kappa|\,|\lambda|\,c_{\varphi_y} + \frac{3i\left(-1+e^{2i\varphi_\omega}\right)|\kappa|\,|\lambda|\,s_{\varphi_y}}{1+e^{2i\varphi_\omega}} + \frac{\left(v^2\,|\lambda|^2 - M_W^2 + M_{H^\pm}^2\right)s_{2\beta}}{v_s^2}\right)$$
$$+ \left(\frac{1}{2}\,|\lambda|\,c_\beta s_\beta\left(\frac{3i\left(-1+e^{2i\varphi_\omega}\right)s_{\varphi_y}}{1+e^{2i\varphi_\omega}} - c_{\varphi_y}\right)v^2 + v_s\left(\frac{\sqrt{2}e^{i\varphi_\omega}\mathrm{Re}A_\kappa}{1+e^{2i\varphi_\omega}} + 4\,|\kappa|\,v_s\right)\right)\delta^{(1)}|\kappa| + \frac{1}{4}v^2 s_{2\beta}\left(\frac{|\lambda|\,s_{2\beta}v^2}{v_s^2} - |\kappa|\,c_{\varphi_y}\right.$$
$$\left. + \frac{3i\left(-1+e^{2i\varphi_\omega}\right)|\kappa|\,s_{\varphi_y}}{1+e^{2i\varphi_\omega}}\right)\delta^{(1)}|\lambda| + \frac{\sqrt{2}e^{i\varphi_\omega}\,|\kappa|\,v_s\delta^{(1)}\mathrm{Re}A_\kappa}{1+e^{2i\varphi_\omega}} + \frac{\left(i - ie^{2i\varphi_\omega}\right)\delta^{(1)}t_{a_s}}{e^{2i\varphi_\omega}v_s + v_s}$$
$$+ \frac{\delta^{(1)}t_{h_s}}{v_s} + \left(-\frac{|\lambda|^2 c_\beta^2 s_\beta^2 v^4}{v_s^3} - \frac{\left(M_{H^\pm}^2 - M_W^2\right)s_{2\beta}^2 v^2}{2v_s^3} + |\kappa|\left(\frac{\sqrt{2}e^{i\varphi_\omega}\mathrm{Re}A_\kappa}{1+e^{2i\varphi_\omega}} + 4\,|\kappa|\,v_s\right)\right)\delta^{(1)}v_s$$
$$+ \frac{\left(-6e^{2i\varphi_\omega}\,|\kappa|\,|\lambda|\,c_\beta s_\beta s_{\varphi_y}v^2 - i\sqrt{2}e^{i\varphi_\omega}\left(-1+e^{2i\varphi_\omega}\right)|\kappa|\,\mathrm{Re}A_\kappa v_s\right)\delta^{(1)}\varphi_\omega}{\left(1+e^{2i\varphi_\omega}\right)^2} \tag{C.161}$$

$$\left(\delta^{(1)}M_{hh}\right)_{h_s a} = \frac{\delta^{(1)}t_{a_d}}{s_\beta v_s} - \frac{1}{2}v\,|\kappa|\,|\lambda|\,v_s c_{\varphi_y}\delta^{(1)}\varphi_y - \frac{1}{2}v\,|\lambda|\,v_s\delta^{(1)}|\kappa|s_{\varphi_y} - \frac{1}{2}v\,|\kappa|\,v_s\delta^{(1)}|\lambda|s_{\varphi_y} - \frac{1}{2}v\,|\kappa|\,|\lambda|\,\delta^{(1)}v_s s_{\varphi_y}$$
$$- \frac{1}{2}\,|\kappa|\,|\lambda|\,v_s\delta^{(1)}vs_{\varphi_y} \tag{C.162}$$

$$\left(\delta^{(1)}M_{hh}\right)_{h_s a_s} = -\frac{2vc_\beta\delta^{(1)}t_{a_d}}{v_s^2} + \frac{2\delta^{(1)}t_{a_s}}{v_s} - 2v^2\,|\kappa|\,|\lambda|\,c_\beta^2 c_{2\beta}s_{\varphi_y}\delta^{(1)}t_\beta - 2v^2\,|\lambda|\,c_\beta s_\beta\delta^{(1)}|\kappa|s_{\varphi_y}$$
$$- 2v^2\,|\kappa|\,c_\beta s_\beta\delta^{(1)}|\lambda|s_{\varphi_y} - 2v^2\,|\kappa|\,|\lambda|\,c_\beta s_\beta c_{\varphi_y}\delta^{(1)}\varphi_y - 4v\,|\kappa|\,|\lambda|\,c_\beta s_\beta\delta^{(1)}vs_{\varphi_y} \tag{C.163}$$

$$\left(\delta^{(1)}M_{hh}\right)_{aa} = v^2\,|\lambda|\,\delta^{(1)}|\lambda| + v\,|\lambda|^2\,\delta^{(1)}v - \delta^{(1)}M_W^2 + \delta^{(1)}M_{H^\pm}^2 \tag{C.164}$$

$$\left(\delta^{(1)}M_{hh}\right)_{aa_s} = \frac{vc_{2\beta}c_\beta^2\delta^{(1)}t_\beta\left(v^2\,|\lambda|^2 - 2M_W^2 + 2M_{H^\pm}^2\right)}{2v_s} - \frac{v\delta^{(1)}v_s\left(6\,|\kappa|\,|\lambda|\,v_s^2 c_{\varphi_y} + s_{2\beta}\left(v^2\,|\lambda|^2 - 2M_W^2 + 2M_{H^\pm}^2\right)\right)}{4v_s^2}$$
$$+ \delta^{(1)}v\left(\frac{s_{2\beta}\left(3v^2\,|\lambda|^2 - 2M_W^2 + 2M_{H^\pm}^2\right)}{4v_s} - \frac{3}{2}\,|\kappa|\,|\lambda|\,v_s c_{\varphi_y}\right) + \delta^{(1)}|\lambda|\left(\frac{v^3\,|\lambda|\,c_\beta s_\beta}{v_s} - \frac{3}{2}v\,|\kappa|\,v_s c_{\varphi_y}\right)$$
$$- \frac{3}{2}v\,|\lambda|\,v_s\delta^{(1)}|\kappa|c_{\varphi_y} + \frac{3}{2}v\,|\kappa|\,|\lambda|\,v_s s_{\varphi_y}\delta^{(1)}\varphi_y - \frac{c_\beta^3\delta^{(1)}t_{h_u}}{v_s} - \frac{vc_\beta s_\beta\delta^{(1)}M_W^2}{v_s} + \frac{vc_\beta\delta^{(1)}M_{H^\pm}^2 s_\beta}{v_s} - \frac{s_\beta^3\delta^{(1)}t_{h_d}}{v_s} \tag{C.165}$$

$$\left(\delta^{(1)}M_{hh}\right)_{a_s a_s} = -\frac{vs_\beta\delta^{(1)}t_{h_u}c_\beta^4}{v_s^2} + \frac{v^2 s_\beta^2\delta^{(1)}M_{H^\pm}^2 c_\beta^2}{v_s^2} - \frac{v^2 s_\beta^2\delta^{(1)}M_W^2 c_\beta^2}{v_s^2} + \frac{1}{2}v^2 c_{2\beta}\left(3\,|\kappa|\,|\lambda|\,c_{\varphi_y}\right.$$
$$\left. - \frac{9i\left(-1+e^{2i\varphi_\omega}\right)|\kappa|\,|\lambda|\,s_{\varphi_y}}{1+e^{2i\varphi_\omega}} + \frac{\left(v^2\,|\lambda|^2 - 2M_W^2 + 2M_{H^\pm}^2\right)s_{2\beta}}{v_s^2}\right)\delta^{(1)}t_\beta c_\beta^2 - \frac{3i\left(-1+e^{2i\varphi_\omega}\right)v\delta^{(1)}t_{a_d}c_\beta}{\left(1+e^{2i\varphi_\omega}\right)v_s^2}$$
$$- \frac{vs_\beta^4\delta^{(1)}t_{h_d}c_\beta}{v_s^2} + \frac{3}{2}v^2\,|\kappa|\,|\lambda|\,s_\beta\left(-\frac{3i\left(-1+e^{2i\varphi_\omega}\right)c_{\varphi_y}}{1+e^{2i\varphi_\omega}} - s_{\varphi_y}\right)\delta^{(1)}\varphi_y c_\beta + \delta^{(1)}v\left(\frac{2\,|\lambda|^2\,c_\beta^2 s_\beta^2 v^3}{v_s^2} + 3\,|\kappa|\,|\lambda|\,c_\beta s_\beta\left(c_{\varphi_y}\right.\right.$$
$$\left.\left. - \frac{3i\left(-1+e^{2i\varphi_\omega}\right)s_{\varphi_y}}{1+e^{2i\varphi_\omega}}\right)v + \frac{\left(M_{H^\pm}^2 - M_W^2\right)s_{2\beta}^2 v}{2v_s^2}\right) + \left(\frac{3}{2}v^2\,|\lambda|\,c_\beta s_\beta\left(c_{\varphi_y} - \frac{3i\left(-1+e^{2i\varphi_\omega}\right)s_{\varphi_y}}{1+e^{2i\varphi_\omega}}\right)\right.$$
$$\left. - \frac{3\sqrt{2}e^{i\varphi_\omega}\mathrm{Re}A_\kappa v_s}{1+e^{2i\varphi_\omega}}\right)\delta^{(1)}|\kappa| + \frac{1}{4}v^2 s_{2\beta}\left(\frac{|\lambda|\,s_{2\beta}v^2}{v_s^2} + 3\,|\kappa|\,c_{\varphi_y} - \frac{9i\left(-1+e^{2i\varphi_\omega}\right)|\kappa|\,s_{\varphi_y}}{1+e^{2i\varphi_\omega}}\right)\delta^{(1)}|\lambda|$$
$$- \frac{3\sqrt{2}e^{i\varphi_\omega}\,|\kappa|\,v_s\delta^{(1)}\mathrm{Re}A_\kappa}{1+e^{2i\varphi_\omega}} + \frac{3i\left(-1+e^{2i\varphi_\omega}\right)\delta^{(1)}t_{a_s}}{\left(1+e^{2i\varphi_\omega}\right)v_s} + \frac{\delta^{(1)}t_{h_s}}{v_s}$$
$$+ \left(-\frac{v^2\left(v^2\,|\lambda|^2 - 2M_W^2 + 2M_{H^\pm}^2\right)s_{2\beta}^2}{4v_s^3} - \frac{3\sqrt{2}e^{i\varphi_\omega}\,|\kappa|\,\mathrm{Re}A_\kappa}{1+e^{2i\varphi_\omega}}\right)\delta^{(1)}v_s$$
$$+ \frac{3e^{i\varphi_\omega}\,|\kappa|\left(6e^{i\varphi_\omega}\,|\lambda|\,c_\beta s_\beta s_{\varphi_y}v^2 + i\sqrt{2}\left(-1+e^{2i\varphi_\omega}\right)\mathrm{Re}A_\kappa v_s\right)\delta^{(1)}\varphi_\omega}{\left(1+e^{2i\varphi_\omega}\right)^2}. \tag{C.166}$$

Appendix D: Neutrino-sneutrino contributions to the h_u-like Higgs self-energy

In this section we present approximate expressions for the h_u-like self-energy. We have used several assumptions which are mentioned in the following. For simplicity, we take $(y_\nu)_{ij} = y_\nu \delta_{ij}$, $(\mu_X)_{ij} = \mu_X \delta_{ij}$, $(\lambda_X)_{ij} = \lambda_X \delta_{ij}$, $(A_\nu)_{ij} = A_\nu \delta_{ij}$, $(A_X)_{ij} = A_X \delta_{ij}$, $(A_e)_{ij} = A_e \delta_{ij}$, $(B_{\mu_X})_{ij} = B_{\mu_X} \delta_{ij}$, $(\tilde{m}_L)_{ij} = \tilde{m}_L \delta_{ij}$, $(\tilde{m}_N)_{ij} = \tilde{m}_N \delta_{ij}$, $(\tilde{m}_X)_{ij} = \tilde{m}_X \delta_{ij}$, $(\tilde{m}_E)_{ij} = \tilde{m}_E \delta_{ij}$, and assume that $\tilde{m}_X = \tilde{m}_N$. Moreover, we restrict ourselves to the CP-conserving case where additionally $\mu_X, B_{\mu_X}, \tilde{m}_X, \tilde{m}_N, \tilde{m}_L, A_\nu \gg v$, the couplings y_ν and λ are small, and $\lambda_X \ll y_\nu, \lambda$. We use the $\overline{\text{DR}}$ renormalization scheme for M_W, M_Z and $M_{H^\pm}$. Excluding the contribution from the NMSSM without seesaw mechanism, we obtain the new contributions from the inverse seesaw mechanism to the renormalized self-energy of the h_u-like Higgs in the vanishing external momentum limit

$$\begin{aligned}\hat{\Sigma}_{h_u h_u}(0) \supset\ & \frac{3c_\beta^4 y_\nu^2}{8\pi^2}\mu_X^2 \log\left(\frac{\mu_X^2}{\mu_R^2}\right) \\ & - \frac{3\alpha_+ y_\nu^2}{512\pi^2} m_{\tilde{n}_+}^2 \log\left(\frac{m_{\tilde{n}_+}^2}{\mu_R^2}\right) \\ & - \frac{3\alpha_- y_\nu^2}{512\pi^2} m_{\tilde{n}_-}^2 \log\left(\frac{m_{\tilde{n}_-}^2}{\mu_R^2}\right) \\ & + \frac{3y_\nu^2}{256\pi^2}\left[16c_\beta^4\left(\tilde{A}_\nu^2 + \tilde{m}_L^2 + \tilde{m}_N^2\right) - \rho\right] \\ & - \frac{3y_\nu^2}{256\pi^2}\log\left(\frac{\tilde{m}_L^2}{\mu_R^2}\right)\left(\frac{16\tilde{\rho}c_\beta^4}{C_\beta M_Z^2}\tilde{m}_L^2 + \rho_1 + \rho_2\right), \end{aligned} \tag{D.167}$$

with $m_{\tilde{n}_\pm}^2 = \tilde{m}_N^2 \pm \mu_X B_{\mu_X} + \mu_X^2$, $\tilde{A}_\nu = A_\nu + \lambda v_S t_\beta/\sqrt{2}$, $C_\beta = 19c_{2\beta} + 2c_{4\beta} + c_{6\beta} - 14$, $\mu^2 = \tilde{m}_N^2 + \mu_X^2 - \tilde{m}_L^2$, and

$$\alpha_\pm = 16c_\beta^4 + 16c_\beta^4\frac{(\tilde{A}_\nu \pm \mu_X)^2}{m_{\tilde{n}_\pm}^2 - \tilde{m}_L^2} + C_\beta\frac{M_Z^2(A_\nu \pm \mu_X)^2}{(m_{\tilde{n}_\pm}^2 - \tilde{m}_L^2)^2}, \tag{D.168}$$

$$\overset{(\sim)}{\rho} = C_\beta M_Z^2\frac{(A_\nu^2 + \mu_X^2)\left(\tilde{m}_L^2 - \tilde{m}_N^2 - \mu_X^2\right) + 2\overset{(\sim)}{A}_\nu \mu_X^2 B_{\mu_X}}{(\tilde{m}_L^2 - m_{\tilde{n}_-}^2)(\tilde{m}_L^2 - m_{\tilde{n}_+}^2)}, \tag{D.169}$$

$$\rho_1 = \frac{\mu^2\left[16c_\beta^4\tilde{m}_L^2\left(A_\nu^2 - \tilde{A}_\nu^2 + \mu^2\right) + \rho\left(2\tilde{m}_L^2 + \mu^2\right)\right] - \mu_X^2 B_{\mu_X}^2\left(16c_\beta^4\tilde{m}_L^2 + \rho\right)}{(m_{\tilde{n}_-}^2 - \tilde{m}_L^2)(m_{\tilde{n}_+}^2 - \tilde{m}_L^2)}, \tag{D.170}$$

$$\rho_2 = -\frac{C_\beta M_Z^2\left(\mu_X^2 B_{\mu_X}^2 - \mu^4\right)\left[\tilde{m}_L^2\left(A_\nu^2 + \mu_X^2\right) - \mu_X^2 B_{\mu_X}^2 + \mu^4\right]}{(m_{\tilde{n}_-}^2 - \tilde{m}_L^2)^2(m_{\tilde{n}_+}^2 - \tilde{m}_L^2)^2}. \tag{D.171}$$

In the limit $\mu_X \gg B_{\mu_X}, \tilde{m}_X, \tilde{m}_N, \tilde{m}_L, A_\nu$, the renormalized h_u-like Higgs self-energy is further simplified as follows

$$\begin{aligned}\hat{\Sigma}_{h_u h_u}(0) \supset\ & -\frac{3y_\nu^2}{256\pi^2}\log\left(\frac{\mu_X^2}{\mu_R^2}\right) \\ & \times\left(16c_\beta^4\tilde{A}_\nu^2 + 2C'_\beta\left(\tilde{m}_L^2 + \tilde{m}_N^2\right) + C_\beta M_Z^2\right) \\ & + \frac{3y_\nu^2}{256\pi^2}\left[16c_\beta^4\tilde{A}_\nu\left(\tilde{A}_\nu - 2B_{\mu_X}\right) + 2C'_\beta\left(\tilde{m}_L^2 - \tilde{m}_N^2\right)\right. \\ & \left. + C_\beta M_Z^2\right], \end{aligned} \tag{D.172}$$

with $C'_\beta = 4c_{2\beta} + c_{4\beta} + 3$.

References

1. N. Aghanim et al. [Planck], Astron. Astrophys. **641** (2020), A6 https://doi.org/10.1051/0004-6361/201833910. arXiv:1807.06209 [astro-ph.CO] [erratum: Astron. Astrophys. **652** (2021), C4]
2. P. Fayet, Supergauge invariant extension of the Higgs mechanism and a model for the electron and its neutrino. Nucl. Phys. B **90**, 104–124 (1975)
3. R. Barbieri, S. Ferrara, C.A. Savoy, Gauge models with spontaneously broken local supersymmetry. Phys. Lett. B **119**, 343 (1982)
4. M. Dine, W. Fischler, M. Srednicki, A simple solution to the strong CP problem with a harmless axion. Phys. Lett. B **104**, 199 (1981)
5. H.P. Nilles, M. Srednicki, D. Wyler, Weak interaction breakdown induced by supergravity. Phys. Lett. B **120**, 346 (1983)
6. J. Frere, D. Jones, S. Raby, Fermion masses and induction of the weak scale by supergravity. Nucl. Phys. B **222**, 11 (1983)
7. J. Derendinger, C.A. Savoy, Quantum effects and SU(2) x U(1) breaking in supergravity gauge theories. Nucl. Phys. B **237**, 307 (1984)
8. J.R. Ellis, J. Gunion, H.E. Haber, L. Roszkowski, F. Zwirner, Higgs bosons in a nonminimal supersymmetric model. Phys. Rev. D **39**, 844 (1989)
9. M. Drees, Supersymmetric models with extended Higgs sector. Int. J. Mod. Phys. **A4**, 3635 (1989)
10. U. Ellwanger, M. Rausch de Traubenberg, C.A. Savoy, Particle spectrum in supersymmetric models with a gauge singlet. Phys. Lett. B **315**, 331–337 (1993)
11. U. Ellwanger, M. RauschdeTraubenberg, C.A. Savoy, Higgs phenomenology of the supersymmetric model with a gauge singlet. Z. Phys. C **67**, 665–670 (1995)
12. U. Ellwanger, M. Rausch de Traubenberg, C.A. Savoy, Phenomenology of supersymmetric models with a singlet. Nucl. Phys. B **492**, 21–50 (1997)
13. T. Elliott, S. King, P. White, Unification constraints in the next-to-minimal supersymmetric standard model. Phys. Lett. B **351**, 213–219 (1995)
14. S. King, P. White, Resolving the constrained minimal and next-to-minimal supersymmetric standard models. Phys. Rev. D **52**, 4183–4216 (1995)

15. F. Franke, H. Fraas, Neutralinos and Higgs bosons in the next-to-minimal supersymmetric standard model. Int. J. Mod. Phys. A **12**, 479–534 (1997)
16. M. Maniatis, The Next-to-Minimal Supersymmetric extension of the Standard Model reviewed. Int. J. Mod. Phys. A **25**, 3505–3602 (2010)
17. U. Ellwanger, C. Hugonie, A.M. Teixeira, The Next-to-Minimal Supersymmetric Standard Model. Phys. Rep. **496**, 1–77 (2010)
18. G. Aad et al., Observation of a new particle in the search for the Standard Model Higgs boson with the ATLAS detector at the LHC. Phys. Lett. B **716**, 1–29 (2012)
19. S. Chatrchyan et al., Observation of a new boson at a mass of 125 GeV with the CMS experiment at the LHC. Phys. Lett. B **716**, 30–61 (2012)
20. I. Gogoladze, N. Okada, Q. Shafi, NMSSM and seesaw physics at LHC. Phys. Lett. B **672**, 235–239 (2009)
21. R. Mohapatra, Mechanism for understanding small neutrino mass in superstring theories. Phys. Rev. Lett. **56**, 561–563 (1986)
22. R.N. Mohapatra, J.W.F. Valle, Neutrino mass and baryon-number nonconservation in superstring models. Phys. Rev. D **34**, 1642–1645 (1986)
23. J. Bernabeu, A. Santamaria, J. Vidal, A. Mendez, J. Valle, Lepton flavor nonconservation at high-energies in a superstring inspired Standard Model. Phys. Lett. B **187**, 303–308 (1987)
24. I. Gogoladze, B. He, Q. Shafi, Inverse seesaw in NMSSM and 126 GeV Higgs boson. Phys. Lett. B **718**, 1008–1013 (2013)
25. W. Wang, J.M. Yang, L.L. You, Higgs boson mass in NMSSM with right-handed neutrino. JHEP **07**, 158 (2013)
26. T. Biekötter, S. Heinemeyer, C. Muñoz, Precise prediction for the Higgs-boson masses in the $\mu\nu$ SSM. Eur. Phys. J. C **78**(6), 504 (2018)
27. T. Biekötter, S. Heinemeyer, C. Muñoz, Precise prediction for the Higgs-boson masses in the $\mu\nu$ SSM with three right-handed neutrino superfields. Eur. Phys. J. C **79**(8), 667 (2019)
28. S. Heinemeyer, M.J. Herrero, S. Penaranda, A.M. Rodriguez-Sanchez, Higgs boson masses in the MSSM with heavy Majorana neutrinos. JHEP **05**, 063 (2011)
29. P. Draper, H.E. Haber, Decoupling of the right-handed neutrino contribution to the Higgs mass in supersymmetric models. Eur. Phys. J. C **73**, 2522 (2013)
30. J. Guo, Z. Kang, T. Li, Y. Liu, Higgs boson mass and complex sneutrino dark matter in the supersymmetric inverse seesaw models. JHEP **02**, 080 (2014)
31. E.J. Chun, V.S. Mummidi, S.K. Vempati, Anatomy of Higgs mass in supersymmetric inverse seesaw models. Phys. Lett. B **736**, 470–477 (2014)
32. M. Muhlleitner, D.T. Nhung, H. Rzehak, K. Walz, Two-loop contributions of the order $\mathcal{O}(\alpha_t\alpha_s)$ to the masses of the Higgs bosons in the CP-violating NMSSM. JHEP **1505**, 128 (2015)
33. T. Dao, R. Gröber, M. Krause, M. Mühlleitner, H. Rzehak, Two-loop $\mathcal{O}(\alpha_t^2)$ corrections to the neutral Higgs boson masses in the CP-violating NMSSM. JHEP **08**, 114 (2019)
34. J. Baglio, T.N. Dao, R. Gröber, M.M. Mühlleitner, H. Rzehak, M. Spira, J. Streicher, K. Walz, A new implementation of the NMSSM Higgs boson decays. EPJ Web Conf. **49**, 12001 (2013)
35. J. Baglio, T.N. Dao, M. Mühlleitner, One-loop corrections to the two-body decays of the neutral Higgs bosons in the complex NMSSM. Eur. Phys. J. C **80**(10), 960 (2020)
36. T.N. Dao, M. Muhlleitner, S. Patel, K. Sakurai, One-loop corrections to the two-body decays of the charged Higgs bosons in the real and complex NMSSM. Eur. Phys. J. C **81**(4), 340 (2021)
37. M.C. Gonzalez-Garcia, J.W.F. Valle, Fast decaying neutrinos and observable flavor violation in a new class of majoron models. Phys. Lett. B **216**, 360–366 (1989)
38. W. Grimus, L. Lavoura, The seesaw mechanism at arbitrary order: disentangling the small scale from the large scale. JHEP **11**, 042 (2000)
39. J.A. Casas, A. Ibarra, Oscillating neutrinos and $\mu \to e, \gamma$. Nucl. Phys. B **618**, 171–204 (2001)
40. W. Siegel, Supersymmetric dimensional regularization via dimensional reduction. Phys. Lett. B **84**, 193–196 (1979)
41. D. Stockinger, Regularization by dimensional reduction: consistency, quantum action principle, and supersymmetry. JHEP **03**, 076 (2005)
42. J. Kublbeck, M. Bohm, A. Denner, FeynArts: computer algebraic generation of Feynman graphs and amplitudes. Comput. Phys. Commun. **60**, 165–180 (1990)
43. T. Hahn, Generating Feynman diagrams and amplitudes with FeynArts 3. Comput. Phys. Commun. **140**, 418–431 (2001)
44. F. Staub, From superpotential to model files for FeynArts and CalcHep/CompHep. Comput. Phys. Commun. **181**, 1077–1086 (2010)
45. F. Staub, Automatic calculation of supersymmetric renormalization group equations and self energies. Comput. Phys. Commun. **182**, 808–833 (2011)
46. F. Staub, SARAH 3.2: Dirac gauginos, UFO output, and more. Comput. Phys. Commun. **184**, 1792–1809 (2013)
47. F. Staub, SARAH 4: a tool for (not only SUSY) model builders. Comput. Phys. Commun. **185**, 1773–1790 (2014)
48. R. Mertig, M. Böhm, A. Denner, Feyncalc—computer-algebraic calculation of Feynman amplitudes. Comput. Phys. Commun. **64**(3), 345–359 (1991)
49. V. Shtabovenko, R. Mertig, F. Orellana, New developments in FeynCalc 9.0. Comput. Phys. Commun. **207**, 432–444 (2016)
50. J. Baglio, R. Grober, M. Muhlleitner, D. Nhung, H. Rzehak et al., NMSSMCALC: a program package for the calculation of loop-corrected Higgs boson masses and decay widths in the (complex) NMSSM. Comput. Phys. Commun. **185**(12), 3372–3391 (2014)
51. F. Domingo, S. Paßehr, Towards Higgs masses and decay widths satisfying the symmetries in the (N)MSSM. Eur. Phys. J. C **80**(12), 1124 (2020)
52. M. Mühlleitner, D.T. Nhung, H. Ziesche, The order $\mathcal{O}(\alpha_t\alpha_s)$ corrections to the trilinear Higgs self-couplings in the complex NMSSM. JHEP **12**, 034 (2015)
53. K. Ender, T. Graf, M. Muhlleitner, H. Rzehak, Analysis of the NMSSM Higgs boson masses at one-loop level. Phys. Rev. D **85**, 075024 (2012)
54. T. Graf, R. Grober, M. Muhlleitner, H. Rzehak, K. Walz, Higgs boson masses in the complex NMSSM at one-loop level. JHEP **10**, 122 (2012)
55. T.N. Dao, L. Fritz, M. Krause, M. Mühlleitner, S. Patel, Gauge dependences of higher-order corrections to NMSSM Higgs boson masses and the charged Higgs decay $H^\pm \to W^\pm h_i$. Eur. Phys. J. C **80**(3), 292 (2020)
56. A. Denner, H. Eck, O. Hahn, J. Kublbeck, Feynman rules for fermion number violating interactions. Nucl. Phys. B **387**, 467–481 (1992)
57. A. Denner, Techniques for calculation of electroweak radiative corrections at the one loop level and results for W physics at LEP-200. Fortsch. Phys. **41**, 307–420 (1993)
58. A. Freitas, D. Stockinger, Gauge dependence and renormalization of tan beta in the MSSM. Phys. Rev. D **66**, 095014 (2002)
59. A. Dabelstein, Fermionic decays of neutral MSSM Higgs bosons at the one loop level. Nucl. Phys. B **456**, 25–56 (1995)
60. A. Dabelstein, The one loop renormalization of the MSSM Higgs sector and its application to the neutral scalar Higgs masses. Z. Phys. C **67**, 495–512 (1995)
61. P. Bechtle, D. Dercks, S. Heinemeyer, T. Klingl, T. Stefaniak, G. Weiglein, and J. Wittbrodt, HiggsBounds-5: Testing Higgs Sectors in the LHC 13 TeV Era. 6 (2020)

62. P.Z. Skands et al., SUSY Les Houches accord: interfacing SUSY spectrum calculators, decay packages, and event generators. JHEP **07**, 036 (2004)
63. P. Bechtle, S. Heinemeyer, O. Stål, T. Stefaniak, G. Weiglein, *HiggsSignals*: confronting arbitrary Higgs sectors with measurements at the Tevatron and the LHC. Eur. Phys. J. C **74**(2), 2711 (2014)
64. F. Capozzi, E. Di Valentino, E. Lisi, A. Marrone, A. Melchiorri, A. Palazzo, Global constraints on absolute neutrino masses and their ordering. Phys. Rev. D **95**, 096014 (2017)
65. S. Parke, M. Ross-Lonergan, Unitarity and the three flavor neutrino mixing matrix. Phys. Rev. D **93**(11), 113009 (2016)
66. M.E. Peskin, T. Takeuchi, Estimation of oblique electroweak corrections. Phys. Rev. D **46**, 381–409 (1992)
67. P. Zyla et al., Review of particle physics. PTEP **2020**(8), 083C01 (2020)
68. C. Patrignani et al., Review of particle physics. Chin. Phys. C **40**(10), 100001 (2016)
69. L. Calibbi, G. Signorelli, Charged lepton flavour violation: an experimental and theoretical introduction. Riv. Nuovo Cim. **41**(2), 71–174 (2018)
70. L. Lavoura, General formulae for f(1) $\to$ f(2) γ. Eur. Phys. J. C **29**, 191–195 (2003)
71. L. Hue, L. Ninh, T. Thuc, N. Dat, Exact one-loop results for $l_i \to l_j\gamma$ in 3-3-1 models. Eur. Phys. J. C **78**(2), 128 (2018)
72. A. Denner et al., Standard Model input parameters for Higgs physics. LHCHXSWG-INT-2015-006 (2015)
73. S.F. King, M. Muhlleitner, R. Nevzorov, Nucl. Phys. B **860**, 207–244 (2012). https://doi.org/10.1016/j.nuclphysb.2012.02.010 arXiv:1201.2671 [hep-ph]
74. T.N. Dao, M. Gabelmann, M. Mühlleitner, H. Rzehak, Two-loop $\mathcal{O}((\alpha_t + \alpha_\lambda + \alpha_\kappa)^2)$ corrections to the Higgs boson masses in the CP-violating NMSSM. arXiv:2106.06990
75. S. Mandal, R. Srivastava, J.W.F. Valle, Electroweak symmetry breaking in the inverse seesaw mechanism. JHEP **03**, 212 (2021)
76. E. Arganda, M.J. Herrero, X. Marcano, C. Weiland, Imprints of massive inverse seesaw model neutrinos in lepton flavor violating Higgs boson decays. Phys. Rev. D **91**, 015001 (2015)